Freezing out fluctuations in Hydro+ near the QCD critical point

Maneesha Pradeep,[1] Krishna Rajagopal,[2] Mikhail Stephanov,[1] and Yi Yin[3]
[1]*Department of Physics, University of Illinois at Chicago, Chicago, Illinois 60607, USA*
[2]*Center for Theoretical Physics, Massachusetts Institute of Technology, Cambridge, Massachusetts 02139, USA*
[3]*Quark Matter Research Center, Institute of Modern Physics, Chinese Academy of Sciences, Lanzhou, Gansu 073000, China*

(Received 3 May 2022; accepted 2 August 2022; published 19 August 2022)

We introduce a freeze-out procedure to convert the critical fluctuations in a droplet of quark-gluon plasma (QGP) that has, as it expanded and cooled, passed close to a posited critical point on the phase diagram into cumulants of hadron multiplicities that can subsequently be measured. The procedure connects the out-of-equilibrium critical fluctuations described in concert with the hydrodynamic evolution of the droplet of QGP by extended hydrodynamics, known as Hydro+, with the subsequent kinetic description in terms of observable hadrons. We introduce a critical scalar isoscalar field sigma whose fluctuations cause correlations between observed hadrons due to the couplings of the sigma field to the hadrons via their masses. We match the QGP fluctuations obtained by solving the Hydro+ equations describing the evolution of critical fluctuations before freeze-out to the correlations of the sigma field. In turn, these are imprinted onto correlations and fluctuations in the multiplicity of hadrons, most importantly protons, after freeze-out via the generalization of the familiar half-century-old Cooper-Frye freeze-out prescription which we introduce. The proposed framework allows us to study the effects of critical slowing down and the consequent deviation of the observable predictions from equilibrium expectations quantitatively. We also quantify the suppression of cumulants due to conservation of baryon number. We demonstrate the procedure in practice by freezing out a Hydro+ simulation in an azimuthally symmetric and boost invariant background that includes radial flow discussed in Rajagopal *et al.* [Phys. Rev. D **102**, 094025 (2020)].

DOI: 10.1103/PhysRevD.106.036017

I. INTRODUCTION

Understanding the physics of strongly interacting matter in extreme conditions and mapping the phase diagram of QCD has been a major goal of theoretical and experimental efforts from high-energy heavy-ion collisions to neutron star mergers [1–3]. One possible central feature of the phase diagram of quantum chromodynamics (QCD)—a QCD critical point at the baryon chemical potential μ_B above which the crossover via which cooling quark-gluon plasma (QGP) becomes ordinary hadronic matter becomes a first order phase transition—still remains a theoretical conjecture. The challenge of its discovery is being taken up by the current Beam Energy Scan (BES) program at the Relativistic Heavy Ion Collider (RHIC) at Brookhaven National Laboratory as well as at planned facilities worldwide. The intriguing hints observed in the first phase of the BES [1,4], in particular the deviations of certain measures of fluctuations from their noncritical baseline, deviations that vary nonmonotonically as a function of $\sqrt{s}$, motivate the ongoing experimental efforts in its second, higher statistics, phase (BES II). BES II data has been taken by the STAR collaboration over the course of 2019-2021 in AuAu collisions at a sequence of collision energies, which corresponds to a scan in μ_B [5,6]. The data is currently being analyzed and we look forward with considerable anticipation to learning much from these measurements.

On the theory side, there have been many studies of the observable consequences of critical fluctuations in heavy ion collisions that produce a droplet of QGP that cool close to a critical point upon making the (greatly simplifying, but unrealistic) assumption that these fluctuations stay in equilibrium [3,5–13]. A part of the essence of critical fluctuations is that since their correlation length, ξ, grows near the critical point, the typical timescale for their evolution grows also—this is referred to as critical slowing down. This means that in the rapidly cooling droplets of QGP produced in heavy ion collisions critical fluctuations

cannot be described by their equilibrium values slaved to hydrodynamic fields. Fortunately, much progress has also been achieved in describing the *nonequilibrium* evolution of hydrodynamic fluctuations [14–43], whose distinctive behavior at long wavelengths is governed by the universality of critical behavior and thus can serve as a signature of the critical point. The challenge which still needs to be addressed is establishing a connection between the hydrodynamic fluid—including its critical fluctuations—and the observed particle yields—and their fluctuations. This work is aimed at closing this gap.

Traditionally one thinks of hydrodynamics as a deterministic theory of fluid evolution. The hydrodynamic variables are the local fluid velocity $u(x)$ as well as *average* densities of conserved quantities like the energy density ϵ and the baryon number density n, or, equivalently, the corresponding conjugate variables such as the temperature T and chemical potentials (like the chemical potential for baryon number, μ_B) characterizing the local equilibrium conditions. These variables evolve deterministically according to hydrodynamic equations. Heavy ion collision experiments, of course, do not measure these hydrodynamic or thermodynamic quantities directly. The conversion to experimentally observable hadron multiplicities occurs at freeze-out—a point in the evolution of the expanding cooling droplet of matter where the density becomes low enough that the kinetic description in terms of a hadron gas becomes applicable and the scattering rates for processes that modify the particle species (i.e., chemical) composition is negligible. At that point one can convert the hydrodynamic variables into particle yields and momentum distributions, i.e., spectra. The well-known procedure known as Cooper-Frye freeze-out [44] maps the local fluid velocity $u(x)$ and hydrodynamic fields such as $T(x)$ and $\mu_B(x)$ on the freeze-out surface (a hypersurface in spacetime) to a simplified hadronic description in terms of kinetic variables of an expanding ideal resonance gas of hadrons, namely a gas of particles with momenta distributed according to boosted Fermi-Dirac or Bose-Einstein distributions. The interactions are encoded in resonances, which later decay, modifying the distributions ultimately measured by experiment. The average densities of conserved quantities such as energy or baryon number are guaranteed to match as long as the hadron resonance gas provides a good description of the equation of state, including the relations between T and μ_B and ϵ and n in that regime.

The Cooper-Frye freeze-out procedure [44] has been successfully employed in the description of high energy heavy-ion collision data for more than four decades to describe average particle yields and spectra. The procedure ensures that the event-averaged baryon number and energy-momentum densities are matched between the hydrodynamic and kinetic theory descriptions. At sufficiently high collision energies $\sqrt{s}$, the data from many experiments are in reasonable agreement with this description across a broad kinematic regime. The Cooper-Frye framework, however, does not describe fluctuations in either the hydrodynamic fluid or the kinetic theory particles. Our goal is to extend the Cooper-Frye procedure to the description of critical fluctuations. Such a description is crucial in the special case of heavy ion collisions that freeze out in the vicinity of a critical point. In this case, fluctuations are both enhanced and of considerable interest, since it is via detecting critical fluctuations that we hope to discern the presence of a critical point [5,6]. These fluctuations are due to thermal noise and their magnitude, or more importantly, their correlations are a sensitive signature of the proximity of a thermodynamic singularity, such as the critical point. Obviously, we cannot expect to match these critical fluctuations using a *free* gas of hadrons. The effect of the critical correlations can be captured by a critical scalar field, which we call σ—a collective mode which becomes "soft," long-range correlated and slow, at the critical point, justifying its treatment as a collective field. One can then match the singular part of fluctuations of hydrodynamic variables by the fluctuation of the field σ which, via its coupling to the observed particles, causes their masses to fluctuate at the time of freeze-out and consequently yields observable fluctuations in particle multiplicities.

In this paper we show how to implement such a procedure and demonstrate its application in a model of the hydrodynamic evolution near the critical point already studied in Ref. [14].

Our paper is organized as follows. In the remainder of this Introduction, in Sec. I A we review some foundational aspects of critical fluctuations in equilibrium and of critical slowing down. We also introduce the Hydro+ equations that describe the dynamics of out-of-equilibrium fluctuations near a critical point. In Sec. I B we review the standard Cooper-Frye freeze-out procedure that neglects fluctuations. With this groundwork in place, in Sec. II, we derive and explain our freeze-out procedure that extends the Cooper-Frye approach so as to match the critical fluctuations just before freeze-out, as described by Hydro+, to observable fluctuations in particle multiplicities just after. In Sec. III we apply our freeze-out procedure to the Bjorken scenario: a fluid that is undergoing boost-invariant longitudinal expansion, meaning that it is cooling, but that is translation-invariant and at rest in the transverse directions. In this simplified setting, we are able to push much of the calculation through analytically and in so doing gain intuition and elucidate general features that arise again in the next section. In Sec. IV we illustrate the use of the freeze-out procedure that we have introduced and fully exercise its salient features by obtaining the two-point correlations of particle multiplicities from the more realistic Hydro+ simulation of Ref. [14] in which the fluid is boost invariant and azimuthally symmetric but is finite in

transverse extent and thus exhibits radial flow. We conclude in Sec. V with a summary of the main qualitative lessons that we draw from our results of Secs. III and IV as well as a look ahead at important next steps.

A. Equilibrium fluctuations, critical slowing down, and evolution equations for out-of-equilibrium fluctuations near a critical point

Thermodynamic equilibrium systems near a critical point are characterized by a certain singular behavior of fluctuations. Due to the divergence of the correlation length ξ the overall magnitude of fluctuations diverges in the thermodynamic limit $V \gg \xi^3$, where V is the system volume, as $\xi \to \infty$. The universality of critical behavior means that the leading singular behavior of the magnitude of fluctuations with ξ is insensitive to microscopic details of the physical system for different systems in the same universality class. The QCD critical point falls in the static universality class of the 3D Ising model [45–48], with a single scalar field becoming soft and slow at the critical point.[1] In QCD, the critical field is a linear combination of scalar operators such as the chiral condensate $\langle \bar{q}q \rangle$ and the baryon number density. This means, in particular, that, in equilibrium near the critical point, the kth cumulants of the baryon number density, which are related to the derivatives of pressure P with respect to baryon chemical potential μ_B at fixed temperature T, diverge as certain powers of ξ [8]:

$$\langle \delta n_B^k \rangle_{\mathrm{eq}} = \left(\frac{T}{V}\right)^{k-1} \frac{\partial^k P(T,\mu_B)}{\partial \mu_B^k} \sim \xi^{\frac{k(5-\eta)}{2}-3}, \qquad (1)$$

where $\eta \approx 0.04$ is the well-known Ising critical exponent [47,48]. The smallness of this exponent makes it negligible in practical applications we will be concerned with here. In this paper we shall only be concerned with the variance of particle multiplicities, which is to say we shall only need Eq. (1) with $k = 2$.

The singular behavior of fluctuations predicted by Eq. (1) points the way toward finding signatures of the presence of a critical point in the phase diagram of QCD in heavy-ion collision experiments. As the location of the freeze-out point on the QCD phase diagram, which moves in response to experimentally varying a parameter such as center of mass collision energy $\sqrt{s}$, approaches and then passes the location of the QCD critical point, the magnitude and higher cumulants of fluctuations should show a characteristic nonmonotonic dependence. There are, however, two essential and quite nontrivial steps which must be taken in order to connect the elegant scaling equation (1) to experimental observables.

[1]In a world with massless up and down quarks and, consequently, three massless pion fields, there would be four soft fields at the critical point, which would then be in the $O(4)$ universality class. See Refs. [45,46,49,50] for further discussion.

First, due to the fact that the droplet of matter produced in a heavy-ion collision expands and cools rapidly it is far from being a static thermodynamic system, meaning that nonequilibrium effects on fluctuations must be considered [15,16]; as the temperature of the fluid drops the fluctuations in the fluid do not have time to develop in the way that they would in equilibrium. Furthermore, critical slowing down is an essential feature of physics near a critical point, meaning that the time needed for fluctuations to grow becomes longer the closer one gets to a critical point. This means that nonequilibrium effects on fluctuations become even more important near a critical point than elsewhere. The description of such nonequilibrium effects is provided by an extension of hydrodynamics known as Hydro+ [18] that we shall review briefly in this section.

The second necessary advance arises due to the fact that experimental measurements do not access hydrodynamic variables, such as the densities of conserved quantities arising in Eq. (1), directly. Therefore, a connection needs to be made between such quantities, and their fluctuations, and the experimentally observable multiplicities of protons, pions, etc. In this paper we propose how this can be done via introducing a scalar field σ in the kinetic theory description of the observable hadrons whose fluctuations can be determined via matching to the critical fluctuations of hydrodynamic quantities, and illustrate it using simplified, but realistic, examples.

Hydro+ extends hydrodynamics by considering the evolution of fluctuations of hydrodynamic variables toward their local thermodynamic equilibrium distribution. These fluctuations are characterized by correlation functions. In this paper, both for simplicity and as a necessary first step, we shall focus on the *magnitude* of fluctuations and defer the discussion of non-Gaussianity measures to future work. The magnitude of the fluctuations is characterized by a two-point correlation function. Near the critical point the slowest hydrodynamic mode is the entropy per baryon $\hat{s} \equiv s/n$ and its fluctuations relax on the (parametrically) longest times scale [18]. Thus the nonequilibrium dynamics is most important in this mode. Furthermore, near the critical point, we can imagine mapping the QCD energy density ε and baryon number density n to the 3D Ising entropy density S and Ising magnetization density M or, equivalently, mapping the QCD phase diagram variables T and μ_B to the 3D Ising variables r (reduced Ising model temperature) and h (magnetic field) as set up explicitly in Refs. [51,52], and then determining which combination of ε and n corresponds to the most singular Ising model fluctuations. In practice, though, any combination of S and M has the same leading singular behavior in powers of the correlation length ξ as long as it involves fluctuations of M, and a similar statement applies to any combination of ε and n as long as it involves fluctuations of the entropy per baryon $\hat{s} \equiv s/n$ [18,20]. It therefore suffices to use the fluctuations of $\hat{s}$, which also happens to be the slowest

hydrodynamic mode. We shall match these fluctuations to the leading singular contribution to the fluctuations of the σ field that we shall introduce in Sec. II.

In the local rest frame of the fluid, the equal-time correlation function of $\hat{s}$ can be expressed in terms of its Wigner transform:

$$\phi_{\mathbf{Q}}(x) \equiv \int_{\Delta \boldsymbol{x}} \langle \delta\hat{s}(x_+)\delta\hat{s}(x_-)\rangle e^{i\mathbf{Q}\cdot\Delta\boldsymbol{x}}. \tag{2}$$

Here $x = (x_+ + x_-)/2$ and $\Delta x = x_+ - x_- = (0, \Delta\boldsymbol{x})$ in the local rest frame of the fluid at the point x. The relaxation of this quantity to its local equilibrium value $\bar{\phi}_{\mathbf{Q}}$ is governed by the equation [18]:

$$u(x)\cdot\partial\phi_{\mathbf{Q}}(x) = -\Gamma(\boldsymbol{Q})(\phi_{\mathbf{Q}}(x) - \bar{\phi}_{\mathbf{Q}}(x)). \tag{3}$$

For the purposes of this paper, the equilibrium $\bar{\phi}_{\boldsymbol{Q}}$ can be adequately approximated by the Ornstein-Zernike ansatz[2]

$$\bar{\phi}_{\mathbf{Q}} \approx \frac{c_p/n^2}{1+(Q\xi)^2}, \tag{4}$$

where $Q \equiv |\boldsymbol{Q}|$ and c_p and n are the heat capacity at constant pressure and the baryon number density.

The Q-dependent relaxation rate, Γ, controls how slowly $\phi_{\mathbf{Q}}(x)$ evolves toward its equilibrium value $\bar{\phi}_{\mathbf{Q}}$ via Eq. (3). The leading critical behavior of Γ depends on the dynamic universality class. For the QCD critical point [53], it is the one of model H (liquid-gas critical point) in Halperin and Hohenberg's classification [54], where the linear combination of $\delta\varepsilon$ and δn given by $\delta\hat{s} = (\delta\varepsilon - (w/n)\delta n)/(Tn)$ is the slow, diffusive, scalar mode nonlinearly coupled to diffusive (transverse) momentum modes. At the same level of approximation as in Eq. (4), the leading critical behavior of the relaxation rate in model H is given by [55]:

$$\Gamma(\boldsymbol{Q}) = \frac{2D_0\xi_0}{\xi^3}K(Q\xi), \tag{5}$$

where ξ_0 is a typical value of the correlation length well away from the critical point, D_0 is a constant with the dimensions of length that we shall take as a free parameter, and

$$K(x) \equiv \frac{3}{4}[1 + x^2 + (x^3 - x^{-1})\arctan x]. \tag{6}$$

As we shall demonstrate, the most important property of the critical mode relaxation rate given by Eqs. (5)–(6) is that it vanishes as $Q \to 0$:

$$\Gamma(\boldsymbol{Q}) = \frac{2D_0\xi_0}{\xi}Q^2 + \mathcal{O}(Q^4). \tag{7}$$

This reflects the fact that $\phi_{\boldsymbol{Q}}$ measures the fluctuation of hydrodynamic variables, which are conserved. The relaxation rate of the 2-point correlator of fluctuations is twice the rate of the relaxation of the corresponding mode, whose relaxation is also diffusive with a diffusion coefficient given by

$$D = D_0\frac{\xi_0}{\xi} \tag{8}$$

which vanishes at the critical point, where $\xi \to \infty$. We can think of the parameter D_0 which we introduced as the diffusion constant at some reference point well away from the critical point. A crude estimate for D_0 could be obtained by using [54,55]

$$D_0 \approx \frac{T}{6\pi\eta\xi_0} \approx \frac{2T}{3s(T)\xi_0}, \tag{9}$$

where η and s are the shear viscosity and entropy density, respectively, and where we have taken $\eta \approx s/(4\pi)$. Taking $s(T) = \tilde{s}T^3$ with $\tilde{s} \approx 6$ as is reasonable around $T = T_c$ [56,57] and choosing $T_c = 160$ MeV and $\xi_0 = 0.5$ fm as we shall throughout, we estimate a critical contribution of $D_0 \approx 0.3$ fm. Assuming that the noncritical contribution to D_0 is not too large, we expect $D_0 > 0.3$ fm but not $D_0 \gg 0.3$ fm. To bracket the uncertainty in this estimate, we shall typically illustrate our results by plotting the results obtained from calculations employing $D_0 = 0.25$ fm and $D_0 = 1$ fm.

To elucidate and emphasize the importance of the conservation laws in the dynamics of fluctuations and, consequently, in the experimental signatures of the critical point we shall compare and contrast results obtained using the model H universality class with those which one would have obtained using model A universality class. In the model A universality class, the critical order parameter is *not* a conserved quantity and the relaxation rate of the fluctuations does not vanish as $\boldsymbol{Q} \to 0$. To the same level of approximation as we have been using so far we can utilize the following ansatz for the relaxation rate in model A:

$$\Gamma(\boldsymbol{Q}) = \frac{\Gamma_0\xi_0^2}{\xi^2}(1 + (Q\xi)^2), \qquad \text{(model A)}, \tag{10}$$

where Γ_0 is a constant with the dimensions of rate (1/time) which we can think of as the relaxation rate at a point well away from the critical point where the correlation length is ξ_0.

As the fireball expands, its temperature T drops and the point characterizing the thermodynamic state of the system on the QCD phase diagram moves past the critical point.

[2]While the value of $\bar{\phi}_{\boldsymbol{Q}}$ at $\boldsymbol{Q} = 0$ in Eq. (3) is determined by thermodynamics, the dependence on $\boldsymbol{Q}$ in this expression is an often used approximation which takes into account the nonzero correlation length. A more sophisticated form can be found in Ref. [18].

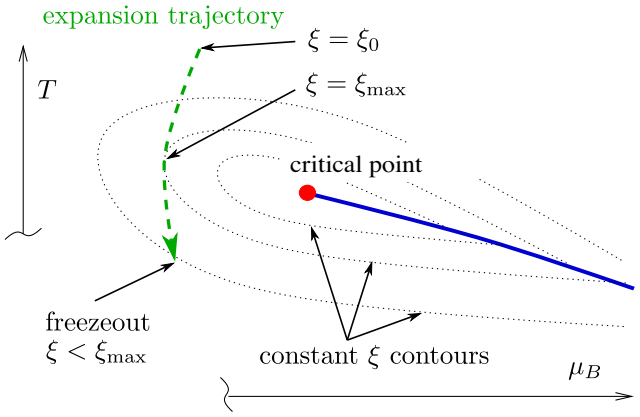

FIG. 1. Schematic view of a trajectory followed by an expanding cooling droplet of matter produced in a heavy ion collision on the QCD phase diagram in the vicinity of the critical point.

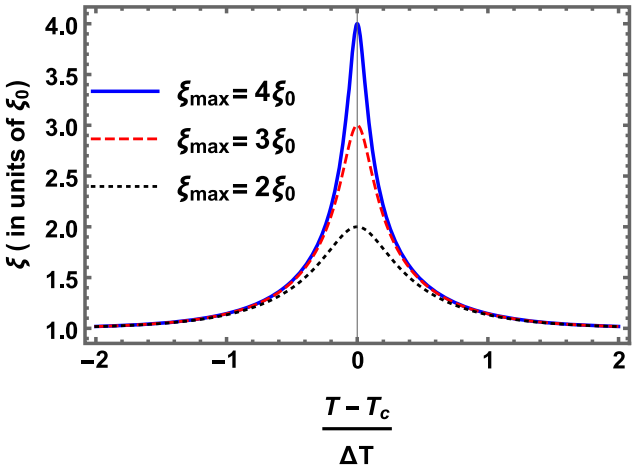

FIG. 2. The dependence of the correlation length ξ on temperature for different trajectories of the fireball expansion (i.e., different $\xi_{\max}$).

The correlation length ξ reaches the maximum value $\xi_{\max}$ (see Fig. 1) which depends on how close the trajectory is to the critical point. The parameter $\xi_{\max}$ is controlled experimentally by varying the collision energy $\sqrt{s}$ [5,6] since collisions with lower $\sqrt{s}$ produce droplets of matter containing a greater excess in the number of quarks over the number of antiquarks, meaning a higher baryon chemical potential μ_B. Lowering the collision energy in steps, as in the BES program at RHIC, moves the entire expansion trajectory in Fig. 1, including the freeze-out point, rightward in steps.

The fluctuation evolution equation (3) depends on the correlation length ξ via the dependence of $\bar{\phi}_{\boldsymbol{Q}}$ and $\Gamma(\boldsymbol{Q})$ on ξ. In a realistic hydrodynamic simulation, ξ will be determined upon solving the hydrodynamic equations with a given equation of state. Since our purpose in this paper is to describe how to freeze out critical fluctuations in hydrodynamics and translate them into observables based on particle multiplicity fluctuations, we shall instead, for simplicity, choose a plausible parametrization of ξ along the expansion trajectory in terms of T.

Specifically, we shall adopt the parametrization of the correlation length along the trajectory of the expanding fireball on the QCD phase diagram in terms of temperature used previously in Ref. [14]:

$$\left(\frac{\xi}{\xi_0}\right)^{-4} = \tanh^2\left(\frac{T - T_c}{\Delta T}\right)\left[1 - \left(\frac{\xi_{\max}}{\xi_0}\right)^{-4}\right] + \left(\frac{\xi_{\max}}{\xi_0}\right)^{-4}, \tag{11}$$

with $\Delta T = T_c/5$. We shall not attempt to refine this parametrization in this work. Alternate parametrizations for the correlation length are discussed, e.g., in Refs. [10,30]. The ansatz in Eq. (11) reflects the main features of $\xi(T)$ relevant for this work—the correlation length reaches a maximum value $\xi_{\max}$ at a certain temperature T_c (close to the crossover temperature) and then decreases as the system continues to cool on its way to freeze-out—as shown in Fig. 2 which is how we imagine ξ varying along a trajectory like that illustrated by the green dashed line in Fig. 1. In our explicit calculations, we shall choose $T_c = 160$ MeV and $\xi_0 = 0.5$ fm.

B. Cooper-Frye freeze-out

Hydrodynamics describes hot and dense QCD matter created in heavy-ion collisions in terms of densities of conserved quantities such as energy or baryon charge, or the corresponding thermodynamic variables such as temperature T or baryochemical potential μ_B, as well as the local fluid velocity. Heavy ion collision experiments, on the other hand, measure multiplicities and momentum distributions of particles which emerge from the expanding and cooling droplet of fluid as it breaks up into hadrons. These multiplicities and distributions are well described by a procedure which we shall summarize below known as Cooper-Frye freeze-out [44] which starts from the output of a hydrodynamic simulation.

In the traditional Cooper-Frye procedure, the macroscopic evolution of the conserved charges and fluid velocity field obtained from a hydrodynamic calculation are converted into a microscopic description in terms of particles in a hadron resonance gas model. The freeze-out hypersurface where this switching is done is determined based on some thermodynamic condition for e.g., fixed temperature or energy density. The averages of the conserved densities are equated to those of a hadron resonance gas of particles via the Cooper-Frye formula. Let dS_μ be the differential element pointing along the normal vector to the freeze-out surface. The mean multiplicity of particle species A ($\langle N_A \rangle$) according to the Cooper-Frye formula is given by,

$$\langle N_A \rangle = d_A \int dS_\mu \int Dp_A p^\mu \langle f_A(x,p) \rangle. \tag{12}$$

Here, d_A is the degeneracy of particle species A and Dp_A is the Lorentz invariant measure:

$$Dp_A = 2\frac{d^4p}{(2\pi)^3}\delta(p^2 - m_A^2)\theta(p_0). \tag{13}$$

$\langle f_A \rangle$ is the momentum-dependent particle distribution function which is either taken to be Fermi-Dirac or Bose-Einstein based on the spin and statistics of hadron species A. For simplicity, throughout this paper we shall ignore the spin and statistics and consider $\langle f_A \rangle$ to be the Boltzmann distribution

$$\langle f_A(x,p) \rangle = \exp\left(\frac{-p \cdot u(x) + \mu_A(x)}{T(x)}\right), \tag{14}$$

where $T(x)$, $\mu_A(x)$ and $u(x)$ are the temperature, the chemical potential of species A, and the local fluid velocity at a point x on the freeze-out hypersurface. For mesons, $\mu_A = 0$, while for baryons/antibaryons $\mu_A = \pm\mu_B$, respectively. In addition to ignoring the modification of the distribution function due to spin and statistics, we also ignore further modifications to $\langle f_A \rangle$ due to viscous effects [58–63] in this preliminary study.

In Sec. II we shall turn to describing our extension of the Cooper-Frye procedure that will enable us to translate the output of a Hydro+ simulation, with traditional hydrodynamic variables as well as fluctuations described by $\phi_{\boldsymbol{Q}}(x)$, into particles in a way that faithfully turns the critical fluctuations in the fluid into fluctuations and correlations of the hadrons. We are pursuing this goal within what is often referred to as a deterministic framework for describing the fluctuations: Hydro+ adds new deterministic equations of motion to the equations of hydrodynamics, equations that describe the evolution of quantities that characterize the fluctuations starting with $\phi_{\boldsymbol{Q}}(x)$ that describes their two-point correlation function. Fluctuations can also be described stochastically, where one evolves an ensemble of configurations each with its own realization of the fluctuations [32–42]. It would be natural in a stochastic description to analyze freeze-out via extending the Cooper-Frye procedure in a manner that follows an analogous logic to that we shall employ here, but we leave this to future work.

II. COOPER-FRYE FREEZE-OUT FOR CRITICAL FLUCTUATIONS

The Cooper-Frye freeze-out procedure described in the previous section converted hydrodynamic variables into (event) mean multiplicities. In order to describe the signatures of the QCD critical point we need to be able to describe also the fluctuations and correlations of these multiplicities. We shall now describe a freeze-out procedure which extends Cooper-Frye freeze-out by connecting the fluctuations of hydrodynamic variables to the fluctuations of the particle multiplicities. We shall focus on the fluctuations of the slowest, and thus most out of equilibrium mode—$\hat{s}$. In Hydro+ the two point function of this mode is given by (its Fourier transform) $\phi_{\mathbf{Q}}$. Our goal is to connect it to the two-point correlation function of the multiplicity fluctuation δf

$$f_A(x,p) = \langle f_A(x,p) \rangle + \delta f_A(x,p) \tag{15}$$

where $\langle f_A(x,p) \rangle$ is given by Eq. (14). We shall use the model of critical correlations which incorporates critical fluctuations in the hadronic description via the interaction of the hadrons with a critical σ field. Such a description of critical fluctuations in a hadron gas has been used in equilibrium [6,8,10–13,64–67] as well as with some out-of-equilibrium effects included [68]. In this approach the interaction with the σ field modifies the masses of the hadrons, to linear order in σ, as follows:

$$\delta m_A = g_A \sigma. \tag{16}$$

We define the value of σ as the deviation of the critical field from its equilibrium value and thus, by definition, $\langle \sigma \rangle = 0$. The proportionality constant g_A plays the role of the coupling constant between the hadron species A and the σ field. The critical contribution to the fluctuations of f_A is due to the dependence of the averaged particle distribution function $\langle f_A \rangle$ on the mass, and is given by

$$(\delta f_A(x,p))_\sigma = g_A \frac{\partial \langle f_A(x,p) \rangle}{\partial m_A}\sigma(x), \tag{17}$$

where $\langle f_A \rangle$ is the Boltzmann distribution in Eq. (14). As a result, fluctuations of the σ field translate into fluctuations and correlations between particles, as in

$$\begin{aligned}&\langle \delta f_{A_1}(x_1,p_1)\delta f_{A_2}(x_2,p_2)\rangle \\ &= \langle f_{A_1}(x_1,p_1)\rangle\delta_{1,2} + g_{A_1}g_{A_2}\frac{\partial\langle f_{A_1}(x_1,p_1)\rangle}{\partial m_{A_1}}\frac{\partial\langle f_{A_2}(x_2,p_2)\rangle}{\partial m_{A_2}} \\ &\quad\times\langle\sigma(x_1)\sigma(x_2)\rangle.\end{aligned} \tag{18}$$

Since hydrodynamic variables, such as baryon density, are expressed in terms of momentum space integrals of the particle distribution functions, the correlation functions of hydrodynamic variables are proportional to the correlation functions of the σ field. This reproduces the essential property of fluctuations at the critical point—the critical (most singular at the critical point) contribution of all correlation functions are proportional to the correlator of a single critical scalar field.

Our main focus is on the correlation functions of $\hat{s}$. Universality of critical behavior dictates that in equilibrium this critical contribution to this correlator should be also proportional to the correlator of σ. In this paper we shall also assume that this remains true out of equilibrium. This allows us to connect the correlations of $\hat{s}$ at the end of the Hydro+ evolution to the fluctuations of σ in the kinetic description at freeze-out and consequently to observable fluctuations and correlations of hadron multiplicities.

The equilibrium fluctuations of the critical field are dictated by the universality of critical behavior and are controlled by the probability functional $P = \exp\{-\Omega/T\}$, where $\Omega[\sigma]$ the effective action (or free energy) which can be written for small fluctuations at long wavelengths in an expansion in powers of the field σ and its gradients around its equilibrium value, $\langle\sigma\rangle = 0$, as follows:

$$\Omega(\sigma) = \int d^3x \left[\frac{(\nabla\sigma)^2}{2} + \frac{m_\sigma^2}{2}\sigma^2 + \frac{\lambda_3}{3}\sigma^3 + \frac{\lambda_4}{4}\sigma^4 + \ldots\right]. \quad (19)$$

The equilibrium two-point correlator can be then found from Eq. (19) and is given by

$$\langle\sigma(\boldsymbol{x}_+)\sigma(\boldsymbol{x}_-)\rangle \approx \frac{T}{4\pi|\Delta\boldsymbol{x}|}\, e^{-|\Delta\boldsymbol{x}|/\xi} \quad (20)$$

where $\Delta\boldsymbol{x} = \boldsymbol{x}_+ - \boldsymbol{x}_-$ and $\xi \equiv 1/m_\sigma$ is the correlation length of the σ-field fluctuations. As we shall only be interested in the two-point correlator in this work and as we are neglecting the (small) nonzero value of the critical exponent η, we will be able to neglect the terms of order σ^3 and higher in the expansion (19). The Fourier/Wigner transform of the two-point correlator is then given by

$$\chi_{\boldsymbol{Q}} \equiv \int_{\Delta\boldsymbol{x}} e^{-i\boldsymbol{Q}\cdot\Delta\boldsymbol{x}}\langle\sigma(\boldsymbol{x}_+)\sigma(\boldsymbol{x}_-)\rangle \approx \frac{T\xi^2}{1+(Q\xi)^2}. \quad (21)$$

In the approximate equalities in Eqs. (20) and (21) we ignore loop corrections, which are known to be small in the 3D Ising universality class in which η is small.

We choose the units of length in Eq. (19) so that the value of ξ introduced in Eqs. (19) and (20) matches the value of the correlation length of the thermodynamic fluctuations introduced above, in Sec. I A. The universality of the critical behavior then dictates that the relationship between the two-point correlators of the fluctuating soft mode in the hydrodynamic description of the physics at the freeze-out point and the fluctuating σ-field in the kinetic theory description of the physics at the same point takes the simple form

$$\langle\delta\hat{s}(\boldsymbol{x}_+)\delta\hat{s}(\boldsymbol{x}_-)\rangle = Z\langle\sigma(\boldsymbol{x}_+)\sigma(\boldsymbol{x}_-)\rangle. \quad (22)$$

Equivalently, the Wigner transforms are related via the same proportionality constant Z:

$$\bar{\phi}_{\boldsymbol{Q}} = Z\chi_{\boldsymbol{Q}}. \quad (23)$$

Using Eqs. (4) and (21) we find

$$Z \approx \frac{c_p}{Tn^2\xi^2}. \quad (24)$$

Note that, while both c_p and ξ^2 diverge at the critical point, their ratio is finite in the approximation we are using.[3]

We shall apply the relationship in Eq. (22), or equivalently in Eq. (23), to express the fluctuations of σ at freeze-out also when these fluctuations are out of equilibrium. Although not strictly justifiable by the universality of critical phenomena in equilibrium, it does allow us to match critical fluctuations at the kinetic and hydrodynamic stage in a way which preserves the information about important nonequilibrium effects, including the effects of conservation laws.

We shall thus determine the correlation functions of σ at freeze-out as follows:

$$\langle\sigma(x)\rangle \equiv 0 \quad (25a)$$

$$\langle\sigma(x_+)\sigma(x_-)\rangle = Z^{-1}\langle\delta\hat{s}(x_+)\delta\hat{s}(x_-)\rangle \quad (25b)$$

where Z is a normalization constant which can be obtained by matching the fluctuations obtained in the kinetic description to fluctuations (i.e., susceptibilities) obtained from the QCD equation of state using Eq. (23). Since in this paper our focus is entirely on developing and exploring the implementation of the freeze-out prescription that we introduce to describe fluctuations, we shall take the constants Z in Eq. (25b) and g_A in Eqs. (16)–(18) as given and postpone their determination by matching a particular QCD EoS to future work. We also note that we shall find ways to express our results that are independent of those unknown parameters. Note that there is a subtlety in defining Eq. (25b) relating to the choice of frame in which x_+ and x_- are at equal time; we shall discuss this in Sec. II A.

Due to Eq. (25a), the mean number of particles is unmodified by critical fluctuations and is given by Eq. (12). Integrating the spatial correlations given by Eq. (18) over the full freeze-out hypersurface and using Eq. (25b), we can express the leading critical contribution to the correlator of particle multiplicities N_A and N_B as:

[3]Our approximation sets the critical exponent to its mean-field value $\eta = 0$, which is a good approximation to make for a critical point in the 3D Ising universality class where $\eta \sim 0.04$. If one uses a more sophisticated, non-mean-field equation of state as in, e.g., Ref. [51], and/or more sophisticated form of $\bar{\phi}_{\boldsymbol{Q}}$ and $\chi_{\boldsymbol{Q}}$ as in Ref. [18], the value of the normalization constant will nevertheless be determined by the matching equation (23), which is more general than the approximation in which we have derived it.

$$\langle \delta N_A \delta N_B \rangle_\sigma = \int dS_{\mu,+} \int dS_{\nu,-} J_A^\mu(x_+) J_B^\nu(x_-) Z^{-1} \langle \delta\hat{s}(x_+)\delta\hat{s}(x_-)\rangle \tag{26}$$

$$J_A^\alpha(x_\pm) \equiv g_A d_A \int Dp_A p^\alpha \frac{\partial \langle f_A(x_\pm, p)\rangle}{\partial m_A} \tag{27}$$

with d_A the spin (and/or isospin) degeneracy of the particle species A. The subscript σ in $\langle \delta N_A \delta N_B \rangle_\sigma$ is there to remind us that this is the contribution due to critical fluctuations. The expressions (26) and (27) constitute the central result whose consequences we shall explore over the course of the rest of this paper by making them explicit in simplified settings. Note that the field σ has now done its job and has now disappeared; in (26) and (27) we have a relationship between the critical fluctuations of hydrodynamic variable on the right-hand side of (26) and the correlator of observable particle multiplicities on the left-hand side.

Although we shall not go beyond two-point correlators in our explicit explorations to come, we note with future work in mind that a straightforward generalization of Eq. (26) yields the form

$$\langle \delta N_A^k \rangle_\sigma^c = \int dS_{\mu_1} \ldots \times \int dS_{\mu_k} J_A^{\mu_1}(x_1) \ldots J_A^{\mu_k}(x_k) Z^{-k/2} \langle \hat{s}(x_1) \ldots \hat{s}(x_k)\rangle_c \tag{28}$$

for the critical contribution to the kth cumulant of the multiplicity of particle species A. We have extended the Cooper-Frye procedure in a way that will allow us to see how the critical, i.e., most singular, contribution the two-point correlations of $\hat{s}$ translates into the variance of observed particle multiplicities. We leave continuing onward to higher-point correlations and non-Gaussian cumulants for future work.

Finally, we note that the total variance of the particle multiplicity has an additional noncritical contribution which is usually taken as Poissonian:

$$\langle \delta N_A^2 \rangle = \langle N_A \rangle + \langle \delta N_A^2 \rangle_\sigma. \tag{29}$$

There can certainly be corrections to the noncritical contributions that we represent here by the Poisson distribution. These may arise from global charge conservation [69,70] or initial fluctuations [71], for example, but we shall not discuss them in this work. This work is intended only as a prescription for freezing out the fluctuations near the critical point that encode information about the leading singularity.

A. Toward explicit evaluation

The extended Cooper-Frye procedure that we have derived above involves expressions with a certain formality to them. Noting that sometimes the devil turns out to be found in the details, we shall now begin to take the steps need to turn these expressions into tools that can be used in explicit calculations.

The Wigner transform ϕ_Q, as defined in Eq. (2), involves integration over the hyperplane orthogonal to the 4-vector $u(x)$. That is, the points x_+ and x_- are equal-time points in the rest frame of the fluid at point x, or $\Delta x \cdot u(x) = 0$ However, in general, the freeze-out surface over which the integration in Eq. (26) is to be performed does not necessarily have the property that the points x_+ and x_- are simultaneous in the rest frame of the fluid at the point x. While, for example, this property holds for boost-invariant Bjorken flow, it does not hold for a flow with radial component, such as the one considered in Ref. [14] that we shall analyze in Sec. IV. In order to translate ϕ_Q into the correlator $\langle \delta\hat{s}(x_+)\delta\hat{s}(x_-)\rangle$ in such a case one needs to be able to evolve this correlator not only in time $u \cdot x$ [using Eq. (3)] but also in time *difference* $u \cdot \Delta x$. We shall show below that because this evolution is slow (and especially slow at the critical point) one can neglect the effect of such evolution and can therefore nevertheless express the unequal-time correlator of interest in terms of ϕ_Q.

Let us consider a small region of the freeze-out surface around a point x that lies on the surface and let us assume that the surface is not perpendicular to the 4-vector $u(x)$. This means that freeze-out does not happen simultaneously at all points in this region. Let us denote the velocity of the frame in which this patch of the freeze-out surface is an equal-time surface by β. ($\beta = 0$ for Bjorken flow). If the typical range of the correlator is of order ℓ_*, then the typical value of the time difference $u(x) \cdot \Delta x \sim \beta \ell_*$. The typical scale ℓ_* can be determined by the condition that the relaxation rate $\Gamma(Q_*) \sim D Q_*^2$ of the corresponding modes $Q_* = 1/\ell_*$ is of order the expansion rate $1/\tau$, where D was introduced in Eq. (8). That is, $\ell_* \sim \sqrt{D\tau}$.

The evolution of the correlator $\langle \delta\hat{s}(x_+)\delta\hat{s}(x_-)\rangle$ as a function of the time separation $u \cdot \Delta x$ occurs with the same rate, also of order $\Gamma(Q_*)$. As a result, the correction to the correlator is of order $\Gamma(Q_*) u \cdot \Delta x \sim \beta\sqrt{D/\tau}$. This quantity is small already because τ is a macroscopic scale, while D is microscopic, i.e., $\tau \gg D$. Furthermore, near the critical point, D itself is vanishing: as seen in Eq. (8), it is smaller than the microscopic scale by another factor of ξ_0/ξ.

More formally, let us define a projection of the separation four-vector Δx onto the plane perpendicular to $u(x)$:

$$\Delta x_\perp \equiv \Delta x - [u(x) \cdot \Delta x] u(x). \tag{30}$$

Then we can express the correlator $\langle \delta\hat{s}(x_+)\delta\hat{s}(x_-)\rangle$ in Eq. (26) in terms of ϕ_Q defined in Eq. (2), obtaining

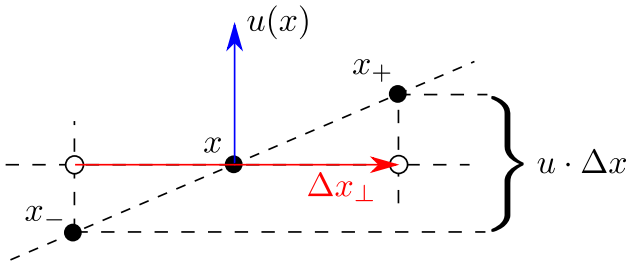

FIG. 3. Geometric representation of Eq. (30). x_+ and x_- are on the freeze-out surface; x is the midpoint between them. The four-vector $\Delta x_\perp$ (red) is perpendicular to the fluid four-velocity at the point x, $u(x)$, meaning that in the local fluid rest frame it is a four-vector with no time-component.

$$\langle \delta\hat{s}(x_+)\delta\hat{s}(x_-)\rangle = \tilde{\phi}(x;\Delta\boldsymbol{x}_\perp) + \mathcal{O}(\sqrt{D/\tau}), \quad (31)$$

where the three-component vector $\Delta\boldsymbol{x}_\perp$ is the projection of the four-vector Δx onto the equal-time hyperplane orthogonal to the vector $u(x)$ as defined in Eq. (30) and illustrated in Fig. 3, and $\tilde{\phi}(x;\Delta\boldsymbol{x}_\perp)$ is the inverse Fourier (Wigner) transform of $\phi_{\boldsymbol{Q}}(x)$:

$$\tilde{\phi}(x;\Delta\boldsymbol{x}_\perp) \equiv \int \frac{d^3Q}{(2\pi)^3} e^{i\boldsymbol{Q}\cdot\Delta\boldsymbol{x}_\perp}\phi_{\boldsymbol{Q}}(x). \quad (32)$$

Equation (31) formalizes the qualitative argument from the preceding paragraph.

We shall be comparing our results with what one would obtain upon assuming the fluctuations are in equilibrium. Up to corrections suppressed by ratios of microscopic (e.g., correlation length ξ) to macroscopic scales (such as hydrodynamic gradient scales, e.g., τ) we can replace the correlation function in Eq. (20) with a delta function:

$$Z^{-1}\langle \delta\hat{s}(\boldsymbol{x}_+)\delta\hat{s}(\boldsymbol{x}_-)\rangle = \langle \sigma(\boldsymbol{x}_+)\sigma(\boldsymbol{x}_-)\rangle = T\xi^2\delta^{(3)}(\Delta\boldsymbol{x}). \quad (33)$$

Substituting into Eq. (26) we find

$$\langle \delta N_A \delta N_B\rangle_\sigma^{\text{eqbm}} = \int dS_\mu(x) J_A^\mu(x)\hat{n}_\nu(x)J_B^\nu(x)T(x)\xi^2(x), \quad (34)$$

where $\hat{n}(x)$ is the unit vector along the normal on the freeze-out hypersurface at x. This expression straightforwardly generalizes existing results for equilibrium fluctuations, see for example Ref. [10], to locally equilibrated fluctuations in a (more realistic) inhomogeneous fireball. We shall make comparisons between our full results and the equilibrium fluctuation predictions (34) in order to highlight the importance of nonequilibrium effects, especially the effects due to conservation laws.

B. Ratios of observables

We shall calculate the contribution of critical fluctuations to the variance of the particle multiplicity of species A (we shall consider protons, $A = p$, and pions, $A = \pi$) in a specified finite rapidity and transverse momentum acceptance window. To eliminate the dependence on the volume (i.e., the transverse size) of the droplet of QGP we shall introduce the intensive ratio

$$\omega_A \equiv \frac{\langle \delta N_A^2\rangle_\sigma}{\langle N_A\rangle}, \quad (35)$$

which was referred to as $\omega_{A,\sigma}$ in Ref. [10]. We note that ω_A depends on the choice of acceptance window. (See, e.g., Ref. [12].) Since this acceptance dependence is not the main focus of the present study, while criticality and nonequilibrium effects are, we shall often illustrate our results by plotting the ratio

$$\tilde{\omega}_A = \frac{\omega_A}{\omega_A^{\text{nc}}}, \quad (36)$$

where ω_A^{nc} is the ω_A calculated upon assuming freeze-out well away from the critical point, i.e., upon setting $\xi_{\max} = \xi_0$. We have checked (for a few sets of parameters) that the acceptance dependence of the numerator and denominator in Eq. (36) is similar and, thus, largely cancels. In contrast, the numerator ω_A is strongly enhanced by critical fluctuations (for example, in equilibrium $\tilde{\omega}_A^{\text{eqbm}} = \xi^2/\xi_0^2$) and is sensitive to the nonequilibrium effects of critical slowing down, while the denominator ω_A^{nc} is, by construction, not affected by critical fluctuations. Although ω_A defined in Eq. (36) depends on the unknown parameters g_A and Z via the ratio $g_A/\sqrt{Z}$, all dependence on these unknowns cancels in the ratio of ratios defined in Eq. (36), within the approximations that we shall make. This is a second significant benefit, and we suggest employing $\tilde{\omega}_A$ (and its generalizations to higher cumulants) in the comparison between future theoretical calculations and experimental measurements.

In subsequent sections, we shall compute $\tilde{\omega}_A$ in two different model hydrodynamic backgrounds. In Sec. III, we study an analytically solvable scenario with longitudinal boost invariance and no dependence on transverse coordinates, which is to say Hydro+ in Bjorken flow. Then, in Sec. IV we shall freeze out the numerical simulation of Hydro+ with azimuthal symmetry, radial expansion, and longitudinal boost invariance from Ref. [14]. Before we conclude this section, though, we need to establish some notation with which to describe two points on the freeze-out hypersurface and the separation between them.

C. Establishing notation for azimuthally symmetric boost invariant freeze-out

To specify the shape of an azimuthally symmetric boost-invariant freeze-out surface, it is convenient to use Bjorken coordinates defined in terms of the Cartesian coordinates (t, x_1, x_2, x_3) in the lab frame via

$$t = \tau\cosh\eta, \quad x_1 = r\cos\varphi, \quad x_2 = r\sin\varphi, \quad x_3 = \tau\sinh\eta. \tag{37}$$

The mutually orthogonal set of unit vectors corresponding to each of the Bjorken coordinates can be expressed in terms of the Cartesian coordinates as

$$\hat{\tau} = (\cosh\eta, 0, 0, \sinh\eta) \tag{38}$$

$$\hat{\eta} = (\sinh\eta, 0, 0, \cosh\eta) \tag{39}$$

$$\hat{r} = (0, \cos\varphi, \sin\varphi, 0) \tag{40}$$

$$\hat{\varphi} = (0, -\sin\varphi, \cos\varphi, 0). \tag{41}$$

The radial profile of a boost-invariant and azimuthally-symmetric freeze-out surface can then be expressed in a parametric form using an arbitrary parameter α as in Ref. [72]

$$\tau = \tau_f(\alpha), \qquad r = r_f(\alpha), \tag{42}$$

so that the point on the freeze-out hypersurface corresponding to parameters α, η, φ is given by:

$$x(\alpha, \eta, \varphi) = \tau_f(\alpha)\hat{\tau}(\eta) + r_f(\alpha)\hat{r}(\varphi). \tag{43}$$

Then, the volume vector normal to the freeze-out hypersurface can be written as $d^3S = nd\alpha\tau d\eta r d\varphi$ where the vector n is given by:

$$n(\alpha, \eta, \varphi) = \frac{\partial x}{\partial\alpha} \wedge \frac{\partial x}{\tau\partial\eta} \wedge \frac{\partial x}{r\partial\varphi} = r_f'(\alpha)\hat{\tau}(\eta) + \tau_f'(\alpha)\hat{r}(\varphi). \tag{44}$$

The flow four-velocity on the freeze-out surface is given by

$$u(\alpha, \eta, \varphi) = u^r(\alpha)\hat{r}(\phi) + u^\tau(\alpha)\hat{\tau}(\eta) \tag{45}$$

in the coordinates with which we are working.

In defining the two-point correlation function we shall need to specify two points on the freeze-out hypersurface. Let $x_\pm \equiv x(\alpha_\pm, \eta_\pm, \varphi_\pm)$ be any two such points on with $x \equiv (x_+ + x_-)/2$ being their midpoint and $\Delta x \equiv x_+ - x_-$ being the separation vector between them. Let us denote similarly $\tau = (\tau_+ + \tau_-)/2, r = (r_+ + r_-)/2, \eta = (\eta_+ + \eta_-)/2, \varphi = (\varphi_+ + \varphi_-)/2$ and $\Delta\tau = \tau_+ - \tau_-, \Delta r = r_+ - r_-, \Delta\eta = \eta_+ - \eta_-, \Delta\varphi = \varphi_+ - \varphi_-$. Then

$$x = \tau\cosh\frac{\Delta\eta}{2}\hat{\tau} + r\cos\frac{\Delta\varphi}{2}\hat{r} + \frac{\Delta\tau}{2}\sinh\frac{\Delta\eta}{2}\hat{\eta} + \frac{\Delta r}{2}\sin\frac{\Delta\varphi}{2}\hat{\varphi} \tag{46a}$$

$$\Delta x = 2\tau\sinh\frac{\Delta\eta}{2}\hat{\eta} + 2r\sin\frac{\Delta\varphi}{2}\hat{\varphi} + \Delta r\cos\frac{\Delta\varphi}{2}\hat{r} + \Delta\tau\cosh\frac{\Delta\eta}{2} \tag{46b}$$

$$u\cdot\Delta x = u^\tau(x)\Delta\tau\cosh\frac{\Delta\eta}{2} - u^r(x)\Delta r\cos\frac{\Delta\varphi}{2} \tag{46c}$$

$$\Delta x_\perp \equiv 2\tau\sinh\frac{\Delta\eta}{2}\hat{\eta} + 2r\sin\frac{\Delta\varphi}{2}\hat{\varphi} + \left[-\Delta\tau u^r(x)\cosh\frac{\Delta\eta}{2} + \Delta r u^\tau(x)\cos\frac{\Delta\varphi}{2}\right] \times (u^r(x)\hat{\tau} + u^\tau(x)\hat{r}), \tag{46d}$$

where $\Delta x_\perp$ was defined in Eq. (30). While the points x_+ and x_- are on the freeze-out surface by construction, the midpoint x, in general, is not. The displacement between the midpoint and the freeze-out surface is, however, small when the typical range of the correlator is much shorter than the typical curvature radius of the freeze-out surface. We can use an argument similar to the one preceding Eq. (30) to simplify the calculation by neglecting the difference between the correlator at the actual midpoint and the correlator at the point on the freeze-out surface given by

$$x \equiv \tau_f(\alpha)\hat{\tau}(\eta) + r_f(\alpha)\hat{r}(\varphi) \tag{47}$$

where $\alpha \equiv (\alpha_+ + \alpha_-)/2$. Henceforth, we shall use x to denote the on-hypersurface approximation (47) to the actual midpoint. Again, neglecting the effect of the curvature and linearizing in $\Delta\eta$, $\Delta\varphi$ and $\Delta\alpha = \alpha_+ - \alpha_-$, the projection of the separation vector $\Delta x_\perp$ from Eq. (46d) onto the hyperplane normal to the four-vector u can be approximated as

$$\Delta x_\perp \approx n\cdot u\Delta\alpha\hat{\alpha}_\perp + \tau_f\Delta\eta\hat{\eta} + r_f\Delta\varphi\hat{\varphi}, \tag{48}$$

where u is the 4-velocity of the fluid at the point x, the vector n is defined in Eq. (44), and we have introduced a spacelike unit vector

$$\hat{\alpha}_\perp \equiv u^r\hat{\tau} + u^\tau\hat{r}. \tag{49}$$

The vectors $\hat{\alpha}_\perp$, $\hat{\eta}$ and $\hat{\varphi}$ form a basis in the hyperplane perpendicular to the four-vector u given by Eq. (45) (the equal-time hyperplane in the rest frame of the fluid at the point x.)

With all of this notation established, we can now take a step toward making the expression Eq. (26) for the squared variance of the multiplicity of species A that we have derived above as our central result more explicit, writing it as

$$\langle(\delta N_A)^2\rangle_\sigma = \int d\alpha_+\tau_+ d\eta_+ r_+ d\varphi_+ \times \int d\alpha_-\tau_- d\eta_- r_- d\varphi_- (n\cdot J_A)_+ (n\cdot J_A)_- \times Z^{-1}\tilde{\phi}(x, \Delta\mathbf{x}_\perp), \tag{50}$$

where $\Delta\mathbf{x}_\perp$ is a three-vector whose components in the $\hat{\alpha}_\perp, \hat{\eta}, \varphi$ basis are given by Eq. (48) and $(n\cdot J_A)_\pm \equiv n(x_\pm)\cdot J_A(x_\pm)$, where n is given by Eq. (44).

The integral in Eq. (27) expressed in Bjorken coordinates takes the form

$$J_A(x_\pm) = \frac{d_A m_A}{T}\int_{y_{\min}}^{y_{\max}}\frac{dy}{2\pi}\int_0^{2\pi} d\phi \times \int_{p_{T,\min}}^{p_{T,\max}}\frac{p_T dp_T}{(2\pi)^2}\langle f_A(x_\pm, p)\rangle \frac{p}{p\cdot u(x_\pm)}, \quad (51)$$

where we used Eq. (14). The Cartesian coordinates in the lab frame of the particle four-momentum are given by

$$p = (m_T\cosh y, p_T\cos\phi, p_T\sin\phi, m_T\sinh y) \quad (52)$$

in terms of the particle rapidity y and transverse mass $m_T \equiv \sqrt{p_T^2 + m^2}$.

III. FREEZING OUT A HYDRO+ SIMULATION WITH BJORKEN FLOW

In this section, we apply our approach to the well-known Bjorken scenario: a hot fluid that is undergoing idealized boost-invariant longitudinal expansion, so that it cools as a function of proper time, but that is translation-invariant and at rest in the transverse directions [73]. We shall obtain some results in this simplified scenario in analytic form, thus allowing us to elucidate general features that we shall observe again in a more realistic scenario with transverse expansion in the next section.

A. Evolution of $\phi_{\boldsymbol{Q}}$

The Bjorken scenario implies that all thermodynamics quantities such as the temperature, T, or the energy density, ε, or net baryon number density, n, as well as quantities describing the fluctuations of these conserved densities depend only on the Bjorken proper time $\tau \equiv \sqrt{t^2 - z^2}$, and are independent of the longitudinal spacetime-rapidity, η, as well as of the transverse coordinates. Thus, the hydrodynamic equations reduce to *ordinary* differential equations for functions of τ which can be solved easily for a given equation of state. Throughout this work, in the Bjorken scenario of this section and in the semirealistic scenario of the next section, we shall employ the simplified equation of state from Ref. [14] that we summarize briefly in Appendix A. Throughout this work, we shall furthermore assume that the dynamical backreaction of the fluctuations on the equation of state and on the hydrodynamic solution is negligible. This assumption has been tested quantitatively in different model calculations [14,30] and is a good approximation: the effects of such backreaction are typically at the subpercent level. The hydrodynamic evolution sets in at $\tau = \tau_i$ where the temperature $T(\tau_i) = T_i$ and it continues until freeze-out at $\tau = \tau_f$ where the temperature $T(\tau_f) = T_f$. In the Bjorken scenario where there is no radial flow, Eq. (45) becomes the statement that the flow velocity unit-four-vector is $u = \hat{\tau}$ in Bjorken coordinates. The evolution equation (3) for the fluctuation measure $\phi_{\boldsymbol{Q}}$ then takes the form of an ordinary differential equation:

$$\partial_\tau \phi_{\boldsymbol{Q}} = -\Gamma(\boldsymbol{Q})(\phi_{\boldsymbol{Q}} - \bar{\phi}_{\boldsymbol{Q}}), \quad (53)$$

where $\Gamma(\boldsymbol{Q})$ depends on τ through $\xi(\tau)$ and is specified via Eqs. (5), (6), and (11). Since our focus throughout is on the effects caused by fluctuations near a critical point, for simplicity we shall assume that the initial fluctuations are in equilibrium, i.e.,

$$\phi_{\boldsymbol{Q}}(\tau_i) = \bar{\phi}_{\boldsymbol{Q}}|_{T=T_i}. \quad (54)$$

This assumption could certainly be improved in the future, but for our present purposes any choice in which the initial fluctuations are small compared to those that develop later will suffice. Since, in the Bjorken scenario, the temperature depends only on τ, the unit four-vector normal to the isothermal freeze-out hypersurface $T(\tau_f) = T_f$ at a spacetime point x is given by $\hat{n}(x) = \hat{\tau}(x) = u(x)$.

In Fig. 4 we plot $\phi_{\boldsymbol{Q}}$ obtained by solving Eq. (53) numerically at three values of τ. In order to highlight the significance of the conservation laws, we compare and contrast the results obtained with two choices of the relaxation rate: model A where $\Gamma(\boldsymbol{Q})$ is as given in Eq. (10) and model H (the universality class of the QCD critical point) where $\Gamma(\boldsymbol{Q})$ is as given by Eq. (5). The most important feature of the model H evolution of $\phi_{\boldsymbol{Q}}$ is the "stickiness" of the $\boldsymbol{Q} = 0$ mode: $\phi_{\boldsymbol{0}}$ remains "stuck" at its initial value, whatever that value is. If the time evolution later takes the fluid along a trajectory that passes near a critical point, $\phi_{\boldsymbol{0}}$ remains stuck in model H whereas in model A it evolves with time, "trying" to follow the dynamics that would have been obtained in equilibrium. The stickiness of $\phi_{\boldsymbol{0}}$ is, obviously, a consequence of the conservation laws in hydrodynamics, since the $Q = 0$ mode corresponds to the fluctuations of conserved quantities (volume integrals of hydrodynamic variables). This important feature is absent in model A result which describes the evolution of fluctuations of quantities which are not conserved.

In Fig. 5 we show the effect of varying the parameter D_0 in the model H relaxation rate (5) on the fluctuation measure $\phi_{\boldsymbol{Q}}$ and its inverse Fourier transform $\tilde{\phi}(\Delta\boldsymbol{x}_\perp)$ defined in Eq. (32) at freeze-out, after Hydro+ evolution from $\tau = \tau_i$ to $\tau = \tau_f$. The large Q, and correspondingly, small Δx (defining $\Delta x \equiv |\Delta\boldsymbol{x}_\perp|$) behavior of the fluctuations is not affected at all, since the fluctuations at short length scales equilibrate quickly. The characteristic Q where the peak of $\phi_{\boldsymbol{Q}}$ is situated shifts to smaller values of Q with increasing D_0 because stronger diffusion tends to

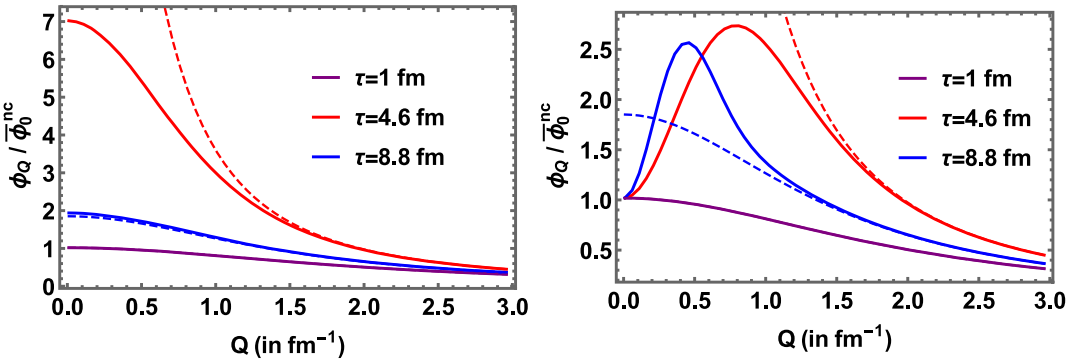

(a) Model A (b) Model H

FIG. 4. Evolution of $\phi_{\boldsymbol{Q}}$ as a function of Bjorken time τ, using model A and model H dynamics, corresponding to the relaxation rates given by Eqs. (10) and (5), respectively. We have taken $\Gamma_0 = 1$ fm^{-1}, $D_0 = 1$ fm and $\xi_{\max} = 3$ fm in both panels. The three solid curves in each figure correspond to different times τ as the boost-invariant, spatially homogeneous, Bjorken fluid is expanding and cooling in the vicinity of a critical point. The temperatures are given by $T = 235$, 160 and 140 MeV, for times $\tau = 1$, 4.6 and 8.8 fm, respectively. The dashed curves represent the equilibrium values $\bar{\phi}_{\boldsymbol{Q}}$ for the corresponding temperatures (times). We have initialized the hydrodynamic solution and the fluctuations at $\tau_i = 1$ fm: at that time $\phi_{\boldsymbol{Q}} = \bar{\phi}_{\boldsymbol{Q}}$ at $T_i = 235$ MeV. The dashed curves are highest at $\tau = 4.6$ fm because that is when the evolution trajectory was closest to the critical point; the fluctuations would be largest at that time if they were in equilibrium. We see that in model H the fluctuations (in our full, out-of-equilibrium, calculation) remain considerably enhanced at $\tau = 8.8$ fm over a range of nonzero values of $\boldsymbol{Q}$. It is evident from the right plot that $\phi_{\boldsymbol{Q}}$ does not evolve at $\boldsymbol{Q} = 0$ in model H. This is a consequence of conservation laws. In both plots, at all times shown, $\phi_{\boldsymbol{Q}}$ and $\bar{\phi}_{\boldsymbol{Q}}$ are both normalized by their noncritical value (their value at a location far enough away from the critical point that $\xi = \xi_0$) at $\boldsymbol{Q} = 0$ in equilibrium, i.e., $\bar{\phi}^{\rm nc}_{\boldsymbol{0}} = ZT\xi_0^2$.

homogenize the system, including fluctuations. This can also be seen in spatial correlator $\tilde{\phi}$ becoming longer ranged. In addition, stronger diffusion (larger D_0) enhances the effect of the critical point on the fluctuations since the system is able to equilibrate more quickly toward the large equilibrium fluctuation values as it passes the critical point on its way to freeze-out. This effect results in a more pronounced (higher) peak in $\phi_{\boldsymbol{Q}}$ and, correspondingly, in an enhancement of $\tilde{\phi}$ at corresponding intermediate values of Δx (of order 3 fm or so).

The conservation laws keep $\phi_{\boldsymbol{Q}}$ stuck at $\boldsymbol{Q} = 0$, which corresponds to keeping the integral of $\Delta x^2\tilde{\phi}$ constant. This means that their effect in panel (b) of Fig. 5 is that if there is a (large, critical) correlation at small Δx they produce a corresponding compensating anticorrelation at longer Δx. One can also show generally that a peak in $\phi_{\boldsymbol{Q}}$ away from $Q = 0$ corresponds to the anticorrelation (i.e., negative tail) in its Fourier transform $\tilde{\phi}(\Delta x_\perp)$. Indeed, if there exist a value of $\boldsymbol{Q}$ at which $\phi_{\boldsymbol{Q}} > \phi_{\boldsymbol{0}}$, then

$$\int d^3\Delta\boldsymbol{x}\tilde{\phi}(\Delta\boldsymbol{x}) < \int d^3\Delta\boldsymbol{x}\cos(\boldsymbol{Q}\cdot\Delta\boldsymbol{x})\tilde{\phi}(\Delta\boldsymbol{x}), \qquad (55)$$

where we used the fact that $\tilde{\phi}(\Delta\boldsymbol{x})$ is an even function. Since $|\cos(\boldsymbol{Q}\cdot\Delta\boldsymbol{x})| \le 1$, the inequality (55) cannot be satisfied if $\tilde{\phi}(\Delta\boldsymbol{x})$ is always positive.

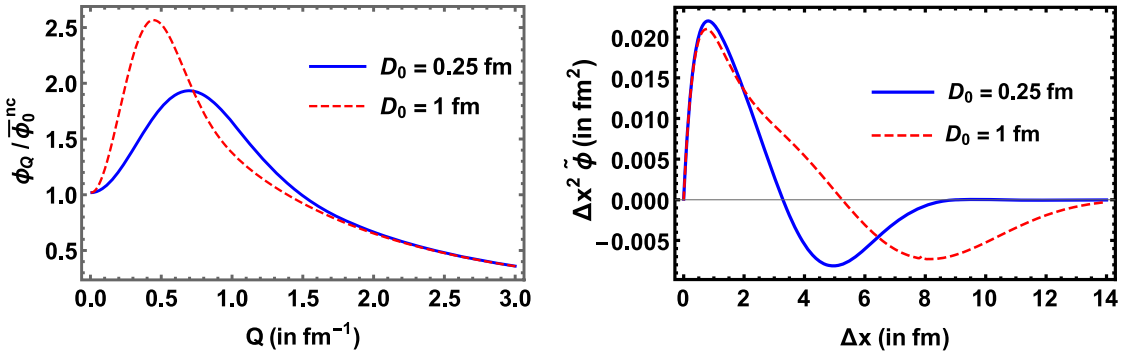

(a) ϕ at freeze-out (b) $\tilde{\phi}$ at freeze-out

FIG. 5. Normalized $\phi_{\boldsymbol{Q}}$ (a) and its inverse Fourier transform $\tilde{\phi}$ (b) at freeze-out $T_f = 140$ MeV after evolution according to model H dynamics with two values of D_0. In the text, we explain the dependence of the shapes of the curves in both panels on D_0, and the consequences of the conservation laws on the shapes of these curves.

B. Multiplicity fluctuations and their rapidity correlator

Upon substituting the solution to Eq. (53), or rather its inverse Fourier transform $\tilde{\phi}$, into Eq. (50), we can now calculate the square variance of multiplicity fluctuations $\langle \delta N_A^2 \rangle$. In the simplified setup that we are employing in this section, we can go one step farther and exploit Bjorken boost invariance to compute explicit results for the rapidity correlator defined as

$$C_A(y_+, y_-) = \left\langle \frac{dN_A}{dy} \right\rangle^{-1} \left\langle \delta \frac{dN_A}{dy_+} \delta \frac{dN_A}{dy_-} \right\rangle_\sigma . \tag{56}$$

(In the next section where we employ a more realistic hydrodynamic solution, we shall only compute $\langle \delta N_A^2 \rangle$, not C_A.) The correlator C_A measures the correlations between the multiplicity of particle species A at rapidities y_+ and y_- and can be determined similarly to Eq. (50) in terms of $\phi_{\boldsymbol{Q}}$ or its inverse Fourier transform $\tilde{\phi}(\Delta \boldsymbol{x}_\perp)$. For the idealized Bjorken scenario, some of the integrals in Eq. (50) (e.g., over transverse coordinates) can be taken analytically. In order to make even further analytical progress we shall consider the case of particles with mass much bigger than the temperature, $m_A \gg T$. This is an adequate approximation for protons and will allow us to perform an additional integral analytically in that case. We shall *not* use this approximation in the next section, where we shall anyway be doing the analogous integrals numerically, but it will be helpful here to make the result and its general features more explicit. As described in detail in Appendix B, upon doing the integrals we obtain

$$\begin{aligned} &\left\langle \delta \frac{dN_A}{dy_+} \delta \frac{dN_A}{dy_-} \right\rangle_\sigma \\ &\quad \approx \frac{g_A^2 d_A^2}{8\pi^{7/2} Z} m_A^{7/2} T_f^{1/2} A_\perp \tau_f^2 \int \frac{d\eta}{\cosh^{5/2}\eta} e^{-\frac{2m_A \cosh\eta}{T_f}} \\ &\qquad \times \int \frac{dQ_\eta}{2\pi} e^{iQ_\eta \tau_f \Delta y} e^{-\frac{Q_\eta^2 \tau_f^2 T_f}{m_A \cosh\eta}} \phi_{\mathbf{Q}_\parallel}(\tau_f) \end{aligned} \tag{57}$$

which is Eq. (B13), where $\mathbf{Q}_\parallel \equiv Q_\eta \hat{\eta}$, $\Delta y \equiv y_+ - y_-$, and $A_\perp$ is the transverse area.

We see that in the simplified setup of this section in which the fluid is translation invariant in the transverse directions, the modes that contribute in Eq. (57) are those whose $\mathbf{Q}$ is directed along the $\hat{\eta}$ direction. Also, the effect of the last Gaussian factor in the Q_η integral in Eq. (57) is to limit the range of that integral to values of order

$$Q_\eta \lesssim \left(\tau_f \sqrt{\frac{T_f}{m_A \cosh\eta}} \right)^{-1} . \tag{58}$$

The fact that the characteristic wavenumber Q of the fluctuations responsible for the correlations at freeze-out is not zero (despite considering a volume of fluid that is infinite in extent in rapidity η in this idealized scenario) is ultimately due to the fact that in the laboratory frame the fireball is not spatially homogeneous: the fluid velocity varies over a longitudinal distance of order τ_f due to the longitudinal expansion. One can check that taking $\tau_f \to \infty$ results in only $Q = 0$ contributing. However, the characteristic Q_η is not just $1/\tau_f$, but rather depends on the mass of the particle. This is due to the thermal smearing, or "blurring," which translates spatial Bjorken rapidity η into kinematic particle rapidity y [12,74]. As we are assuming that $m_A \gg T$, the factor $\sqrt{T_f/(m_A \cosh\eta)}$ in Eq. (58) is the typical thermal rapidity of the particles at temperature $T_f/\cosh\eta$, which can be understood as the freeze-out temperature "redshifted" by longitudinal expansion.

The final piece that we need in order to compute C_A is the denominator in Eq. (56). By explicit calculation starting from Eq. (12), in the Bjorken scenario in which we are working $\langle dN_A/dy \rangle$ is given by:

$$\left\langle \frac{dN_A}{dy} \right\rangle = d_A A_\perp \tau_f (2\pi)^{-2} \int_{m_A}^\infty m_T^2 dm_T \int d\eta e^{-\frac{m_T \cosh\eta}{T_f}} \cosh\eta . \tag{59}$$

Substituting Eqs. (57) and (59) into Eq. (56), we can evaluate C_A which, because of boost invariance, is a function of Δy only. In Fig. 6, we plot our results for C_A, normalized by the its noncritical value at $\Delta y = 0$, $C_A^{\rm nc}(0)$, which we estimate by substituting $\phi_{\boldsymbol{Q}} = ZT(Q^2 + \xi_0^{-2})^{-1}$ into Eq. (57), where ξ_0 is, as before, the correlation length away from critical point defined in Eq. (11). That is, we define the ratio that we have plotted in Fig. 6 as

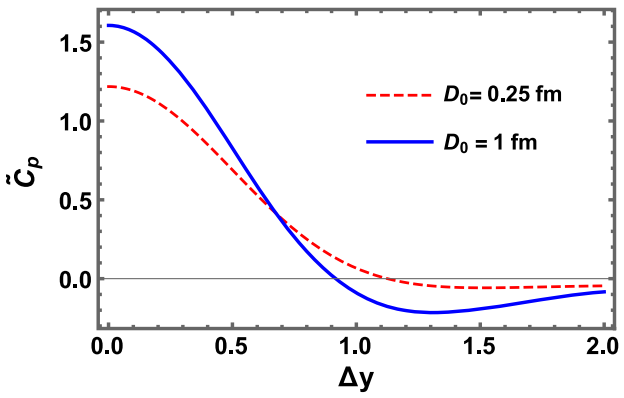

FIG. 6. Normalized proton multiplicity correlator $\tilde{C}(\Delta y)$ for protons from Eq. (60) as a function of the rapidity gap Δy in the Bjorken scenario for two choices of the diffusion parameter D_0.

$$\tilde{C}_A(\Delta y) \equiv \frac{C_A(\Delta y)}{C_A^{\rm nc}(0)}. \tag{60}$$

Since $\xi_{\max} > \xi_0$, critical fluctuations make the ratio $\tilde{C}_A(0)$ larger than unity.

In Fig. 6 we also illustrate the dependence of the rapidity correlations on the value of the diffusion parameter D_0. Stronger diffusion (larger D_0) enhances the effects of the critical point in $\phi_{\boldsymbol{Q}}$, as we saw in Fig. 5. This enhancement is reflected in the corresponding particle rapidity correlations, as seen in Fig. 6 at small Δy. Due to conservation laws, anticorrelations at large Δy are also enhanced. (For any value of D_0, the consequence of conservation is that the integral under the curve $\tilde{C}_A$ over all separations Δy is independent of D_0 and is determined by the initial fluctuations. This means that when we increase D_0 and see $\tilde{C}_A(\Delta y)$ growing at small Δy, it must also become more negative at large Δy.) However, unlike the direct effect of diffusion on the *range* of the spatial correlator $\tilde{\phi}$ in Fig. 5(b), the effect on the *range* of $C(\Delta y)$ in Fig. 6 is minor. This is due to the fact that this range is mostly determined by the effect of thermal rapidity smearing or "blurring" [12].

Now, the variance of the particle multiplicity $\langle \delta N_A^2 \rangle_\sigma$ that in the general case takes the form (50) can in this Bjorken scenario be obtained from the rapidity correlator $C(\Delta y)$ by integration over the rapidity window $y_\pm \in (-y_{\max}, y_{\max})$, i.e.,

$$\frac{\langle \delta N_A^2 \rangle_\sigma}{\langle N_A \rangle} = \int_{-2y_{\max}}^{2y_{\max}} d\Delta y \left(1 - \frac{|\Delta y|}{2y_{\max}}\right) C(\Delta y). \tag{61}$$

Upon using our expression for $C(\Delta y)$ from Eqs. (56), (57), and (59) and using the fact that boost invariance implies that $\langle N_A \rangle = 2y_{\max}\langle dN_A/dy \rangle$, we now obtain the result

$$\begin{aligned}\langle \delta N_A^2 \rangle_\sigma \approx{}& \frac{1}{2} Z^{-1} m_A^{7/2} T_f^{1/2} \pi^{-7/2} g_A^2 d_A^2 A_\perp \tau_f^2 \\ &\times \int d\eta \,\mathrm{sech}^{5/2}\eta\, e^{-\frac{2m_A \cosh\eta}{T_f}} \\ &\times \int \frac{dQ_\eta}{2\pi} \frac{\sin^2(\tau_f Q_\eta y_{\max})}{\tau_f^2 Q_\eta^2} e^{-\frac{Q_\eta^2 \tau_f^2 T}{m_A \cosh\eta}} \phi_{\mathbf{Q}_\parallel}(\tau_f)\end{aligned} \tag{62}$$

The Δy dependence of $C(\Delta y)$ translates into the rapidity acceptance window dependence of $\langle \delta N_A^2 \rangle_\sigma$, which has been discussed in the literature, e.g., in Ref. [12], and will not be discussed here.

C. Dependence of fluctuations on dynamics and on proximity of freeze-out to the critical point

In this paper we focus on the magnitude of fluctuations and their dependence on the proximity of freeze-out to the critical point as well as on the diffusion parameter D_0. The proximity of the freeze-out to the critical point is controlled by two major factors. One is the proximity of the trajectory to the critical point, which in our analysis is quantified by $\xi_{\max}$—the maximum equilibrium correlation length along the expansion trajectory on the phase diagram. The larger the value $\xi_{\max}$, the closer the system has passed to the critical point on its way to freeze-out. The smallest values of $\xi_{\max} \approx \xi_0$ correspond to trajectories furthest away from the critical point, on the edge of the critical region. In Fig. 7, we plot the normalized critical contribution to the squared variance of the proton multiplicity from Eq. (36) on $\xi_{\max}$. One can see the effect of the critical point on the fluctuations at freeze-out increases as the trajectory approaches the critical point (as $\xi_{\max}$ increases).

The other factor controlling the proximity of the critical point to the freeze-out is the freeze-out temperature T_f. The higher the freeze-out temperature is (while still below critical temperature), i.e., the earlier the freeze-out occurs and the closer the freeze-out is to the critical point. Correspondingly, the fluctuations at freeze-out increase with $\xi_{\max}$ as well as with T_f in Fig. 7.

The results in Fig. 7 also demonstrate that the magnitude of the critical point signatures crucially depends on dynamics. As we already discussed in Figs. 5 and 6, stronger diffusion (larger D_0) leads to larger effects of the critical point. We can see this in Fig. 7 by comparing the plots for two different values of D_0. In addition, as a result of the conservation laws the magnitude of fluctuations is significantly smaller than the equilibrium expectation at freeze-out, as can be seen by comparing to panel (c) in Fig. 7. It is also apparent from this comparison that, while the equilibrium expectation in panel (c) depends very strongly on the freeze-out temperature (the higher the temperature the closer is the freeze-out to the critical point, since $T_c > T_f$), the dynamical predictions in panels (a) and (b) of Fig. 7 are much less sensitive to the freeze-out temperature. This can be understood as a "memory" effect: the fluctuations at freeze-out encode some information about fluctuations at earlier times because they do not have time to equilibrate, an effect which is enhanced by critical slowing down. This has the consequence that even though freeze-out happens at a temperature below that of the critical point, effects of critical fluctuations persist until freeze-out and yield signatures in observables. The magnitude of such memory effects depends on the value of D_0. We see that the results of our out-of-equilibrium calculation at freeze-out illustrated in panels (a) and (b) of Fig. 7 arise via an interplay between the suppression of fluctuations relative to their magnitude in equilibrium due to conservation and the enhancement of fluctuations arising from memory effects.

In panel (c) of Fig. 7, the equilibrium magnitude of fluctuations saturates as $\xi_{\max}$ increases and the trajectory followed by the cooling plasma gets closer to the critical point. This happens because the freeze-out occurs at a

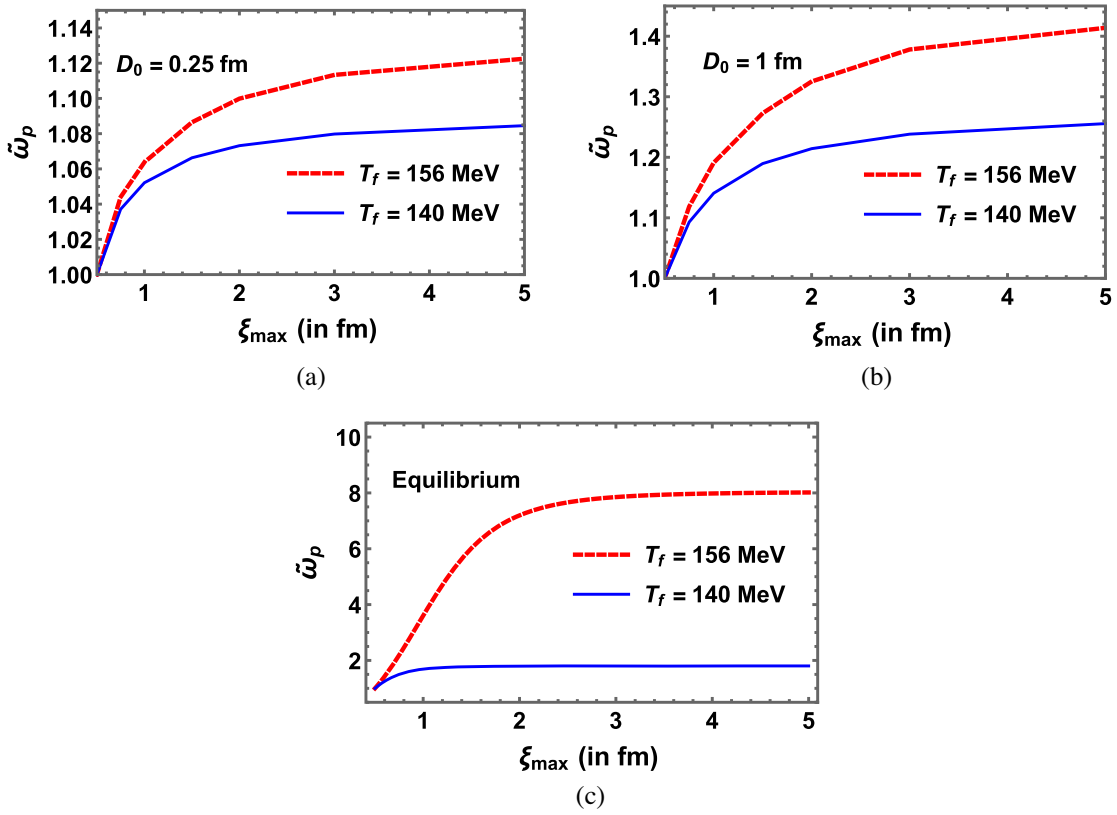

FIG. 7. The normalized fluctuation measure for protons, Eq. (36), as a function of $\xi_{\max}$, the maximum value of the equilibrium correlation length achieved along the system trajectory. Panels (a) and (b) correspond to different diffusion strengths, quantified by D_0, while red and blue curves correspond to different freeze-out temperatures. Panel (c) shows the result that would have been obtained under the assumption that fluctuations are in equilibrium at freeze-out.

temperature T_f below the critical point, where $\xi(T_f) < \xi_{\max}$, and as the trajectory approaches the critical point, $\xi_{\max}$ diverges while $\xi(T_f)$ goes to some (large) constant value which is independent of $\xi_{\max}$ as $\xi_{\max} \to \infty$. The saturation is less pronounced in panels (a) and (b) because of dynamical memory effects: the blue curve "remembers where it was" at earlier times.

To summarize some central results of this section: (i) in the Bjorken scenario considered here there is a clear suppression in the normalized fluctuation measure $\tilde{\omega}_A$ at freeze-out for the values of D_0 considered, because the slow modes are fluctuations of a conserved quantity; (ii) in model H dynamics, $\tilde{\omega}_A$ is less sensitive to the freeze-out temperature than would be the case if the fluctuations were in equilibrium throughout. In the next section, we shall investigate how radial flow modifies these and other observations.

IV. FREEZING OUT A SEMIREALISTIC NUMERICAL HYDRO+ SIMULATION

In this section, we demonstrate the use of the freeze-out procedure introduced in Sec. II and employed in a Bjorken scenario in Sec. III to obtain the two-point correlations of particle multiplicities from the Hydro+ simulation that was introduced and analyzed, but not frozen out, in Ref. [14]. As in the previous section, the system under consideration is boost invariant and has azimuthal symmetry. Unlike in the previous section, the system we consider here is finite in transverse extent and thus exhibits radial flow. We give a brief description of the details of simulation here. For more details the reader may refer to Ref. [14].

The evolution of the energy density, $\varepsilon(r,\tau)$ and the fluid four-velocities $u(r,\tau)$ in our simulation is determined using the standard MIS second order hydrodynamic equations as implemented in the publicly available VH1 + 1 hydrodynamic code [75–77]. The equation of state $p(\varepsilon)$ used in the simulation was introduced in Ref. [14] and was already employed in Sec. III and, for convenience, is reviewed in Appendix A. We set the shear viscosity to entropy density ratio to $\eta/s = 0.08$ throughout, and solve the equations numerically using a spatial (radial) lattice with 1024 points spaced by 0.0123 fm and a time step of 0.005 fm. In this section, we initialize the hydrodynamic simulation at $\tau_i = 1$ fm, with an initial central temperature of 330 MeV, following Ref. [75]. We set the radial flow v_r and the viscous part of the stress-energy tensor $\Pi_{\mu\nu}$ to zero initially at $\tau = \tau_i$. We employ the standard Glauber

model radial profile corresponding to a central Au-Au collision at $\sqrt{s} = 200$ GeV for $\varepsilon(r)$ at $\tau = \tau_i$, again following Ref. [75].

As in Ref. [14], in our Hydro+ simulation the hydrodynamic densities $\varepsilon(r,\tau)$ and $\Pi_{\mu\nu}(r,\tau)$ and the four-velocities $u(r,\tau)$ provide the background for the evolution of the fluctuations described by ϕ_Q according to Eq. (3). Again following Ref. [14], we choose to initialize the fluctuations ϕ_Q at $\tau = \tau_i$ by setting them to the corresponding equilibrium values determined by the local temperature at this initial time, i.e.,

$$\phi_Q(r,\tau_i) = \bar{\phi}_Q|_{T(r,\tau_i)}. \tag{63}$$

For the interested reader, the limitations of the various assumptions made in setting up this Hydro+ simulation, as well as possible future improvements to it, are detailed in Ref. [14].

We calculate the evolution of ϕ_Q using the same code as in Ref. [14], with two important changes. For simplicity, in their pioneering calculation the authors of Ref. [14] chose to simulate the evolution of ϕ_Q according to model A relaxation dynamics, as if the fluctuations were those of a quantity that is not conserved. In this work, as in Sec. III we employ model H dynamics which takes into account conservation laws. This gives us an opportunity to highlight the effects of conservation laws on the dynamics of ϕ_Q and on the resulting particle multiplicity fluctuations by comparing the results of this section to those obtained by repeating the calculations of this section using model A evolution. We perform this comparison in Appendix C. The second change that we make relative to Ref. [14] is that here we shall neglect the back-reaction of the fluctuations on the hydrodynamic densities. The modifications to the bulk dynamics of the hydrodynamic fluid, in particular its entropy density $s(r,\tau)$, introduced by the presence of the fluctuations was computed in Ref. [14,30] and in fact the fluctuations and the hydrodynamic densities were computed self-consistently. However, these authors showed that including backreaction self-consistently introduces fractional changes to $\varepsilon(r,\tau)$ and $v_r(r,\tau)$ that are small, rarely comparable to 1% and typically much smaller. For this reason we neglect these effects.

In the remainder of this section, we demonstrate the implementation of the freeze-out prescription introduced in Sec. II to freeze out the Hydro+ simulation with the background described above for some reasonable values of D_0. After describing and illustrating the evolution of ϕ_Q in Sec. IV A and the fluctuations on the freeze-out surface in Sec. IV B, in Sec. IV C we describe the resulting fluctuations in particle multiplicities.

A. Evolution of ϕ_Q

In this subsection, we present and discuss the space-time dependence of the fluctuation measure ϕ_Q as it evolves according to the relaxation equation given by Eq. (3) with the model H relaxation rate given by Eq. (5). The radial dependence of the flow and temperature profiles makes ϕ_Q dependent on the radial variable r in addition to the Bjorken time τ. Several representative characteristic curves, or flow lines, determined by the flow velocity u, are shown in Fig. 8.

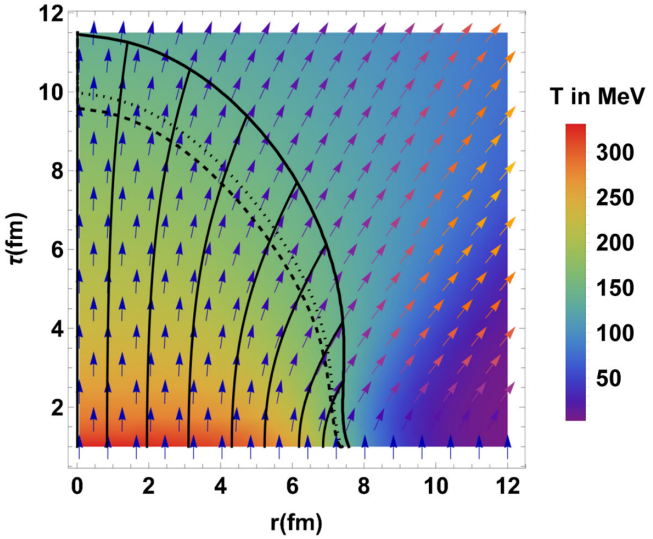

FIG. 8. The space-time dependence of the temperature (represented by color) and flow velocity in the hydrodynamic simulation of the expanding cooling droplet of quark-gluon plasma. The magnitude of the radial flow at each space-time point is indicated by the tilt of the arrows. The dashed, dotted and solid black curves are the isothermal curves at $T = 160$ MeV, 156 MeV and 140 MeV, respectively. Examples of fluid cell trajectories, or hydrodynamic flow lines, are illustrated by solid black lines tangential to local flow vectors.

In Fig. 9, we plot our results for the fluctuation measure ϕ_Q in the hydrodynamic background illustrated in Fig. 8 at three different times τ along two hydrodynamic flow lines, one close to the center of the fireball ($r(\tau_i) = 0.7$ fm) and one further out ($r(\tau_i) = 5$ fm). We display results from simulations performed with $D_0 = 0.25$ fm (slower diffusion) and $D_0 = 1$ fm (faster diffusion) and $\xi_{\max} = 1$ fm (trajectory further away from the critical point) and $\xi_{\max} = 3$ fm (trajectory closer to the critical point). In all the panels, at $\tau = 1$ fm (black curve) ϕ_Q is given by its equilibrium value. In the upper (lower) four panels, the red curves at $\tau = 9.19$ fm ($\tau = 5.14$ fm) are drawn at the time when the fluid cell moving along the flow line that started at $r_i = 0.7$ fm ($r_i = 5$ fm) has cooled to the temperature $T = T_c = 160$ MeV and the blue curves at $\tau = 11.36$ fm ($\tau = 6.72$ fm) are drawn at the time when these fluid cells have cooled further to $T = 140$ MeV. Increasing $\xi_{\max}$, i.e., bringing the evolution trajectory closer to the critical point, causes the magnitude of equilibrium fluctuations to increase. However the relaxation to the equilibrium value becomes slower since its rate $\Gamma(Q) \propto DQ^2$ and

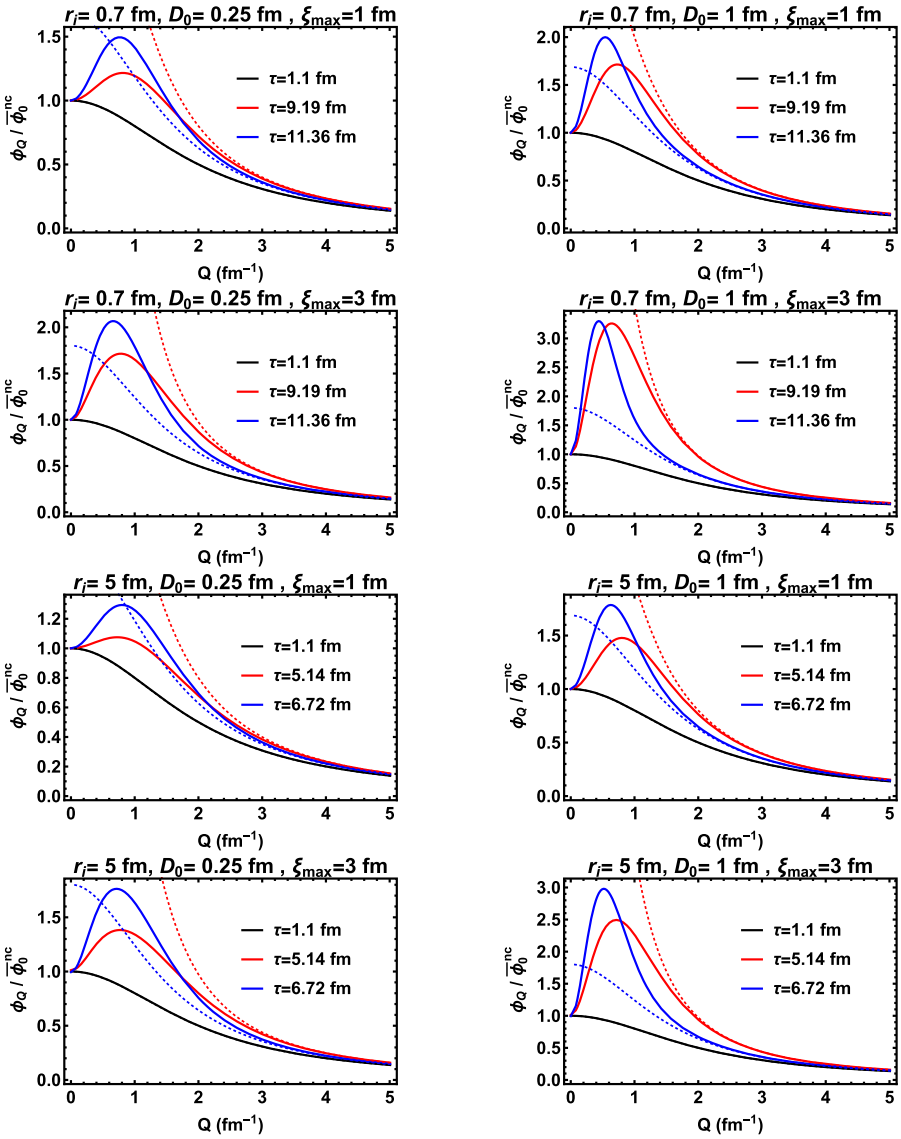

FIG. 9. Hydro+ fluctuation measure ϕ_Q along two hydrodynamic flow lines passing through $r = r_i$ at initial time $\tau = \tau_i$, with $r_i = 0.7$ fm (top four panels) and 5 fm (bottom four panels). The four plots in the left (right) column are for $D_0 = 0.25$ fm ($D_0 = 1$ fm), with $\xi_{\max} = 1$ fm and $\xi_{\max} = 3$ fm in alternating rows. The solid and dashed curves are, respectively, the ϕ_Q and $\bar{\phi}_Q$ (normalized to their values at $Q = 0$ away from the critical point, where $\xi = \xi_0$) at three times τ indicated in the plot legends; the choice of τ's is explained in the text.

$D = D_0\xi_0/\xi$ is proportional to $1/\xi$. We find that the former effect "wins" in the sense that ϕ_Q at the time the fluid cell trajectory cools to $T = 140$ MeV (i.e., the blue curves in Fig. 9), which is well after the fluid cell trajectory passes the point where $\xi = \xi_{\max}$, see Fig. 1, increases with $\xi_{\max}$, at least in the range of the parameters we have considered.

We see by comparing the left and right columns of Fig. 9 that increasing the diffusion parameter D_0, which increases the relaxation rate, has the consequence that ϕ_Q is closer to its instantaneous equilibrium form $\bar{\phi}_Q$ during the course of the evolution. The value of ϕ_Q at $Q = 0$, however, remains invariant during the evolution due to the conservation laws inherent in model H: $\Gamma(Q = 0) = 0$.

The Q-dependence of ϕ_Q is shaped by two competing effects. As a given hydrodynamic cell, represented by a point on the phase diagram (see Fig. 1) moving along the expansion trajectory, approaches the critical point, the "desired" equilibrium values of $\bar{\phi}_Q$, to which ϕ_Q is forced to relax by Eq. (3), increases across all values of Q. However, while at larger Q, the relaxation is fast enough to effectively equilibrate ϕ_Q to these larger equilibrium values, at lower Q conservation laws slow down the evolution, making the ϕ_Q values lag behind $\bar{\phi}_Q$ more significantly. This produces a peak in ϕ_Q at a characteristic value of Q denoted by Q^{peak} in Ref. [30] which moves to lower values of Q as D_0 is increased. These features are

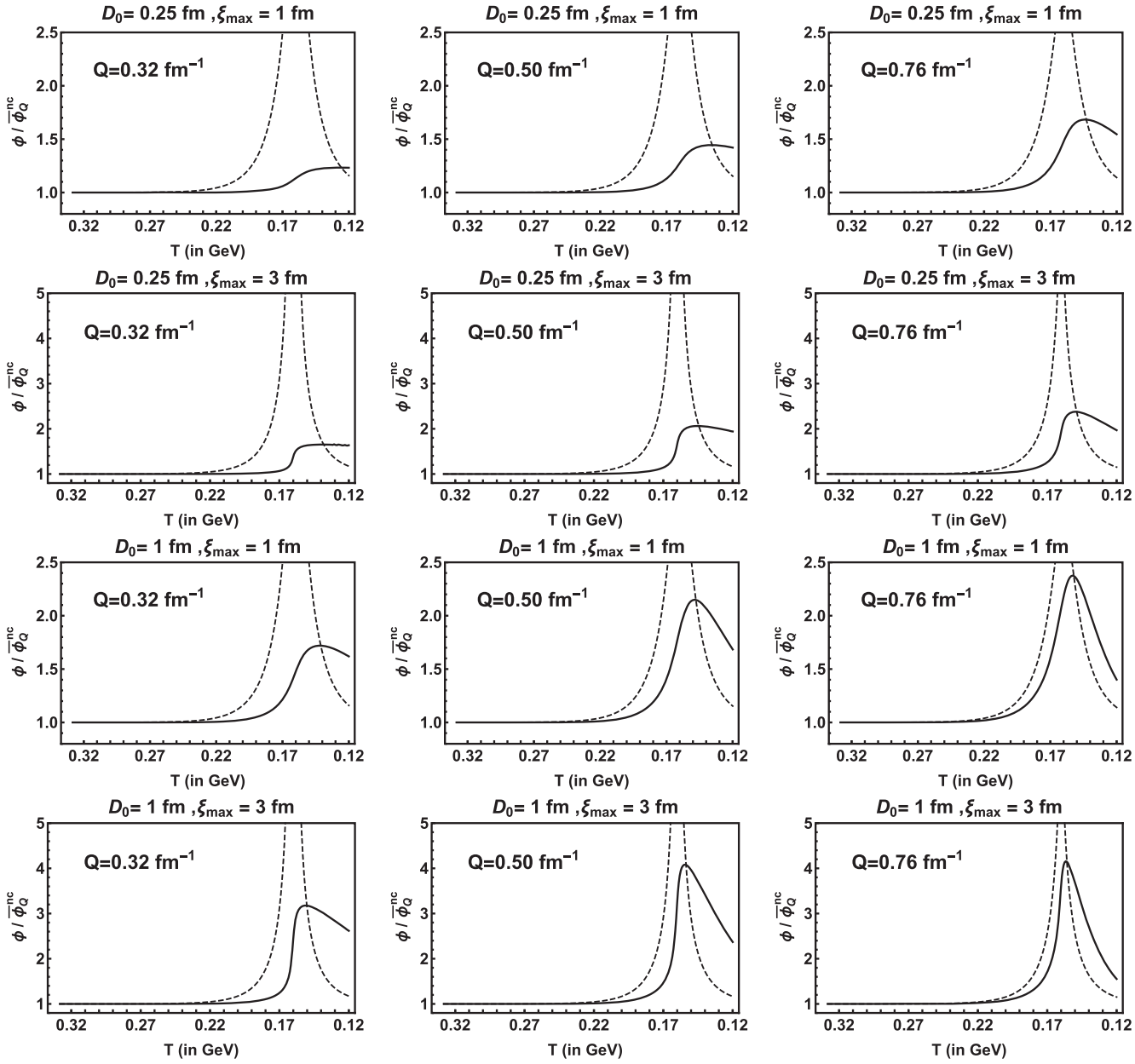

FIG. 10. The values of ϕ_Q (suitably normalized) for three representative values of Q (same for each column), and for values D_0 (same in top and bottom six panels) and $\xi_{\max}$ (same in alternating rows) as in Fig. 9. The values of ϕ_Q are taken along a fluid cell trajectory and plotted as a function of temperature, which is a monotonous function of time τ along the trajectory. The trajectory chosen for these plots begins at $r_i = r(\tau_i) = 1.8$ fm. The dashed and solid curves represent the equilibrium $\bar{\phi}_Q$ and nonequilibrium ϕ_Q, respectively.

evident in Fig. 9 across the range of parameters we have considered. It is also instructive to compare and contrast Fig. 9 with the results that would be obtained if the fluctuations followed model A dynamics where the relaxation rate of low-Q modes is not suppressed and, consequently, $Q^{\text{peak}} = 0$. We perform this comparison in Appendix C; see Fig. 17 from that Appendix which is to be compared with Fig. 9.

In the simpler Bjorken scenario of Sec. III, we described "memory effects" and looked at their dependence on Q and the diffusion parameter D_0. We can do the same here, for the ϕ_Q obtained in this more realistic r-dependent calculation, by displaying our results as in Fig. 10, where suitably normalized ϕ_Q and $\bar{\phi}_Q$ are plotted as a function of the local temperature along a fluid cell trajectory for three different values of Q. In accordance with Eq. (53), the value of ϕ_Q increases when $\phi_Q < \bar{\phi}_Q$ and decreases when $\phi_Q > \bar{\phi}_Q$, as ϕ_Q "tries" to relax toward the rising, and later falling, equilibrium value $\bar{\phi}_Q$, as the critical point is approached and later passed. For larger values of D_0 (as in the bottom half of Fig. 10) the rate of relaxation is

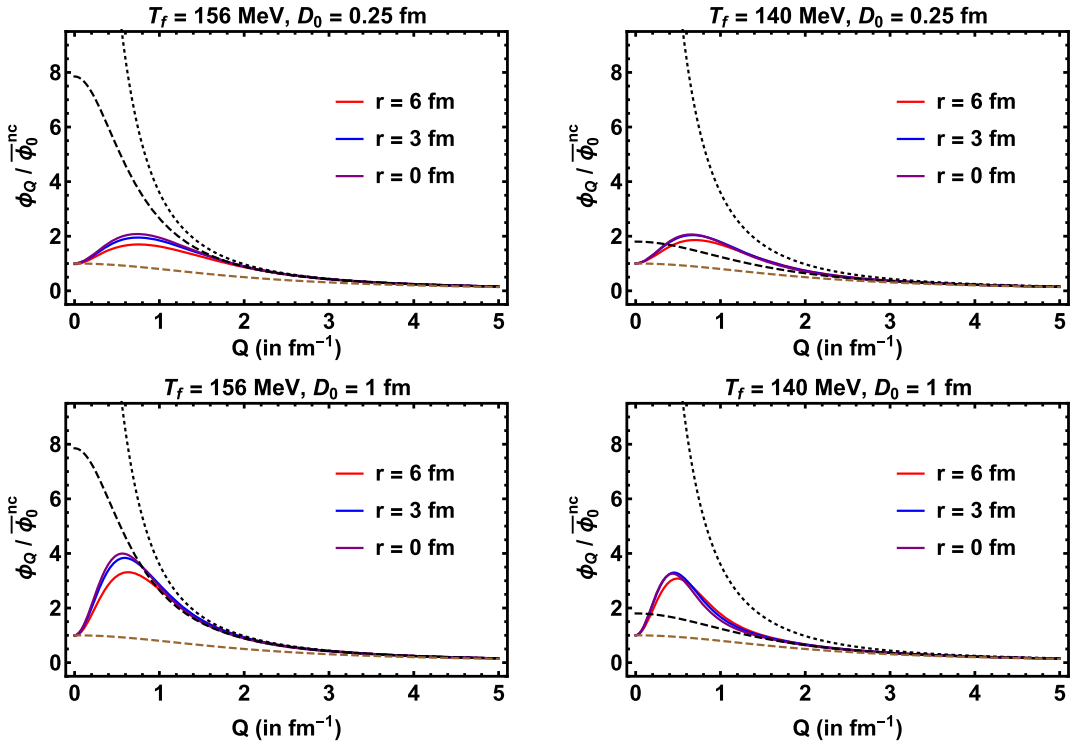

FIG. 11. The Hydro+ variable ϕ_Q (normalized to its value at $Q = 0$ away from the critical point, where $\xi = \xi_0$) at freeze-out evolved with two different diffusion parameters $D_0 = 0.25$ fm (upper panels) and 1 fm (lower panels) and $\xi_{\max} = 3$ fm. The left (right) panels show results for evolution until the decreasing temperature has reached a higher (lower) freeze-out temperature. The blue, red and purple curves show the values of ϕ_Q at different points on the freeze-out hypersurface, characterized by the radial coordinate r. The black dashed and dotted curves are the equilibrium curves at $T = T_f$ and $T = T_c$ respectively. The dashed brown curve is the (noncritical) equilibrium curves corresponding to $\xi = \xi_0$.

greater, meaning that ϕ_Q rises more rapidly, and therefore higher, in the critical region. Although it also drops more rapidly as the temperature drops further, overall a larger D_0 yields larger fluctuations, at least within the reasonable range of values of D_0 that we explore. For small Q (see the left column in Fig. 10), the value of ϕ_Q grows very slowly, and reaches values much lower that the equilibrium $\bar{\phi}_Q$ before it starts decreasing. However, for low Q, the rate at which ϕ_Q decreases after the critical point has been passed is also slow, and as a result significant memory of the fluctuation magnitude near the critical point (albeit itself smaller than equilibrium magnitude) is retained at freeze-out. This dynamics is qualitatively similar to the dynamics first described in Ref. [15] in a very simplified model of the out-of-equilibrium evolution of critical fluctuations with no spatial- or Q-dependence.

B. Fluctuations on the freeze-out surface

As in the Bjorken scenario discussed in Sec. III, we consider two isothermal freeze-out scenarios with $T_f = 140$ MeV and $T_f = 156$ MeV. The main difference here relative to Sec. III is that the temperature is now not only a function of τ but also of the radial coordinate r. An isothermal surface, therefore, is not simply $\tau = \text{const}$ for all r, as in the previous section. The surface $T(\tau, r) = T_f$ can be parametrized according to the discussion in Sec. II C and we use the notations and approximations discussed in that section. For simplicity, we choose the parameter α introduced in Eq. (42) according to $\alpha = r$.

The magnitude of fluctuations at $T = 156$ MeV in equilibrium is several times higher than that at $T_f = 140$ MeV, since $T = 156$ MeV is closer to the critical temperature $T_c = 160$ MeV. However, the time that the system spends in the critical region before freezing out is shorter for $T_f = 156$ MeV than for $T_f = 140$ MeV. By comparing these two freeze-out scenarios, we can understand the sensitivity of out-of-equilibrium fluctuations to the proximity of the freeze-out temperature to the critical point.

In Fig. 11, suitably normalized plots of ϕ_Q are shown for three points on the freeze-out hypersurface, characterized by radial coordinate $r = 0$, 3 and 6 fm, for two choices of freeze-out temperature T_f and two values of the diffusion parameter D_0. These plots of ϕ_Q should be compared to the equilibrium $\bar{\phi}_Q$ at three characteristic points: at $T = T_c$, at $T = T_f$ and at a point far away from critical, where $\xi = \xi_0$, shown by the dashed and dotted curves. The left and right

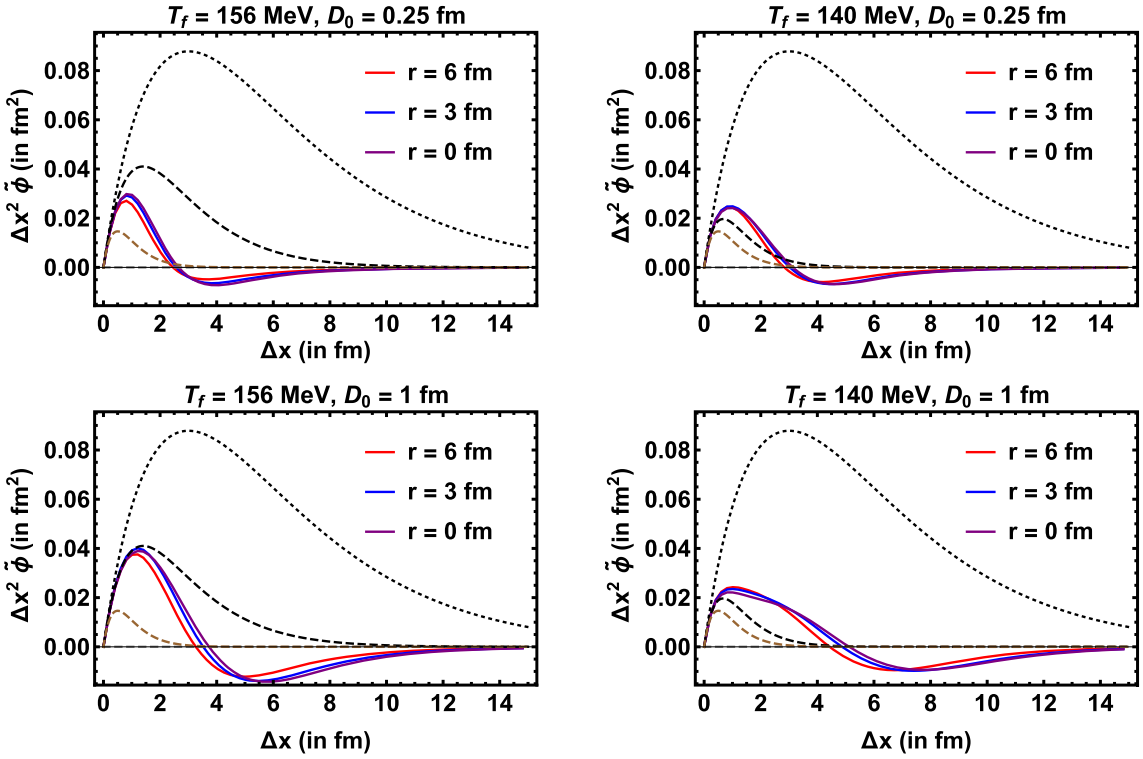

FIG. 12. $\tilde{\phi} \times \Delta x^2$, the measure of fluctuations of $\hat{s}$ described by the correlator $\langle \delta\hat{s}(x_+)\delta\hat{s}(x_-)\rangle$, at freeze-out as a function of the spatial separation between the points $\Delta x \equiv |\Delta \boldsymbol{x}_\perp|$. In the calculations depicted in different panels, the $\phi_{\boldsymbol{Q}}$'s were evolved with two different D_0's until freeze-out at two different T_f's, with the inverse Fourier transform to obtain $\tilde{\phi}(\boldsymbol{x}_\perp)$ performed at T_f. In all panels, we have chosen a trajectory with $\xi_{\max} = 3$ fm. The three r values depicted via the colored curves correspond to three r values on the freeze-out surface in the lab frame. The black dashed and dotted curves are the equilibrium curves at $T = T_f$ and $T = T_c$ respectively. The dashed brown curve is the (noncritical) equilibrium curve corresponding to $\xi = \xi_0$.

plots differ by the choice of the freeze-out temperature, $T_f = 156$ MeV and 140 MeV, respectively. As expected, $Q = 0$ modes are "stuck" at their initial values and are not affected by the critical point. (To see how different this would be in the absence of conservation, Fig. 11 can be compared with the results obtained in the case of model A dynamics in Fig. 18 in Appendix C.) At moderate Q the "memory" effect weakens and at large Q the modes closely track their equilibrium values, which rises and then falls as the critical point is approached and then passed. By comparing the plots in Fig. 11 for different T_f, we can also see that at smaller, but not too small, Q, the "memory" causes the fluctuation measure $\phi_{\boldsymbol{Q}}$ to be larger than its equilibrium value $\bar{\phi}_{\boldsymbol{Q}}$. This effect is more pronounced for lower T_f, due to the fact that the equilibrium fluctuations are smaller there.

Having understood the effects of varying the parameter D_0 and the proximity to the critical point on the fluctuation measure $\phi_{\boldsymbol{Q}}$, as in Sec. III the next step toward the calculation of observable particle multiplicity fluctuations is to compute $\tilde{\phi}(\Delta \boldsymbol{x}_\perp)$, the inverse Fourier transform of $\phi_{\boldsymbol{Q}}$ defined in Eq. (32). In Fig. 12, we plot $\Delta x^2 \tilde{\phi}(\Delta \boldsymbol{x}_\perp)$ as a function of the spatial separation $\Delta x \equiv |\Delta \boldsymbol{x}_\perp|$ between the two points in the correlator $\langle \delta\hat{s}(x_+)\delta\hat{s}(x_-)\rangle$, see Eq. (31). By comparing to Fig. 5(b), we see that the D_0-dependence is qualitatively similar to that in the Bjorken scenario, discussed at length in Sec. III. The small Δx (large Q) behavior of the fluctuations is not affected by changing D_0, while at the same time the spatial correlator becomes longer ranged as D_0 is increased. The correlator goes negative at larger values of Δx; this is a consequence of conservation as can be seen by comparing Figs. 12–19 in Appendix C and as explained in the context of the Bjorken scenario in Eq. (55). Finally, consistent with what we have already seen in Fig. 11, with either value of D_0 memory effects are strong enough that the magnitudes of the fluctuations are not much smaller if the freeze-out temperature is $T_f = 140$ MeV (well below the critical point) as compared to their magnitudes if $T_f = 156$ MeV (very close to $T_c = 160$ MeV) despite the fact that the equilibrium fluctuations at these two temperatures differ substantially.

C. Variance of particle multiplicities

Because of the greater symmetry in the simpler Bjorken scenario that we were employing there, in Sec. III we were able to compute the rapidity correlator $C(\Delta y)$ of the

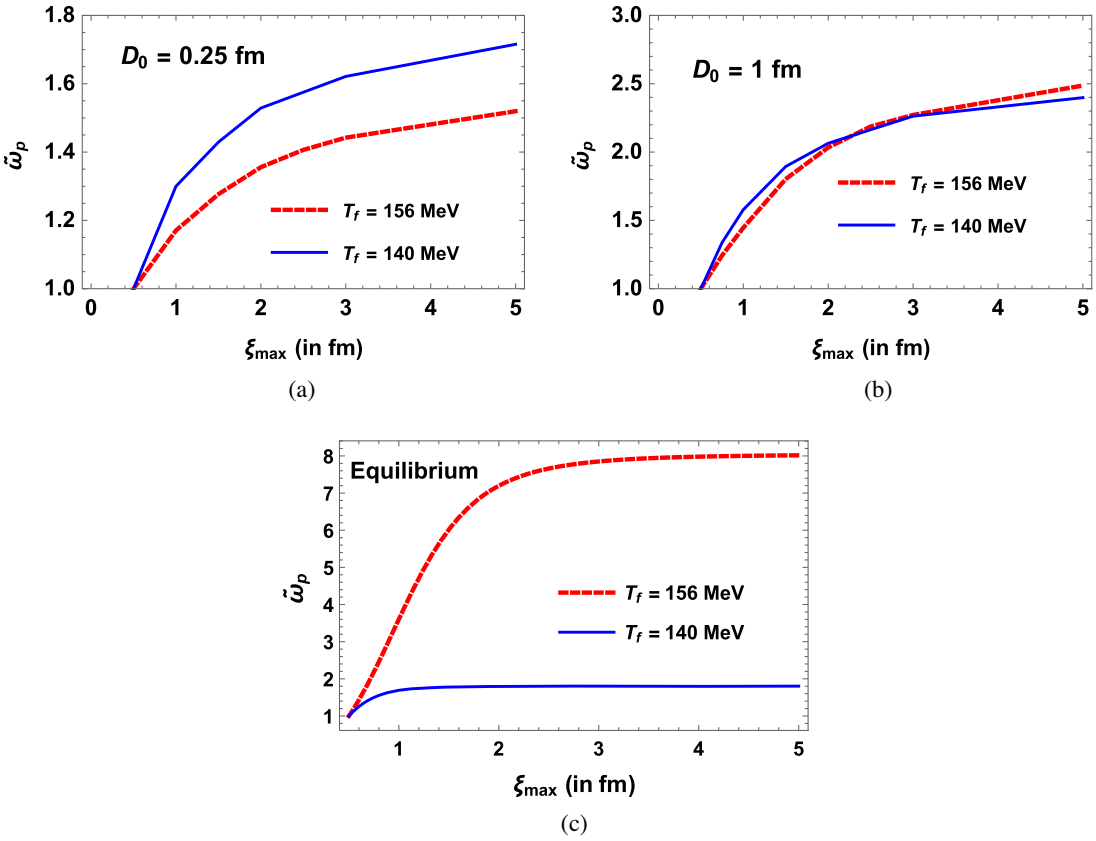

FIG. 13. Normalized measure of the fluctuations in proton multiplicity, $\tilde{\omega}_p = \frac{\omega_p}{\omega_p^{\rm HC}}$, as a function of the maximum equilibrium correlation length along the system trajectory, which is to say as a function of how closely the trajectory passes the critical point. As $D_0 \to \infty$, the $\tilde{\omega}_p$'s approach their equilibrium values shown in panel (c).

multiplicity fluctuations, before integrating over a rapidity window to obtain the variance of the particle multiplicity. Here, with nontrivial radial dependence and radial flow we shall instead obtain the variance of the multiplicity of particles of species A directly from $\tilde{\phi}$ by employing the more general expressions in Eqs. (50) and (51). As we did in Sec. III, we shall compute ω_A, the ratio of the variance of the multiplicity of species A to its mean, see Eq. (35). We can obtain the mean multiplicity of protons and pions for a rapidity acceptance window $[-y_{\max}, y_{\max}]$ and acceptance cuts in p_T using the Cooper-Frye formula

$$\langle N_A \rangle = d_A \int dS_\mu \int_{-y_{\max}}^{y_{\max}} \frac{dy}{2\pi} \int_{p_{T,\min}}^{p_{T,\max}} \frac{p_T dp_T}{2\pi} \int_0^{2\pi} \frac{d\phi}{2\pi} e^{-\frac{p\cdot u}{T_f}} p^\mu, \tag{64}$$

employing the flow velocity $u(x)$ profile and freeze-out hypersurface for the simulation from Ref. [14] illustrated in Fig. 8. The fluctuation measure ω_A is then obtained by taking the ratio of Eqs. (50) and (64). In this subsection, we present the results for the normalized fluctuation measure $\tilde{\omega}_A$ as defined in Eq. (36) as a function of $\xi_{\max}$ (which is to say as a function of how close the trajectory in the phase diagram is to the critical point) for protons and pions obtained with our two choices of D_0 and with our isothermal freeze-out scenario with two different choices of the freeze-out temperature T_f, as discussed above. In all calculations, we choose the acceptance cuts $p_T \epsilon (0.4\ \text{GeV}, 2\ \text{GeV})$ and $y_{\max} = 1$. As already discussed above, $\tilde{\omega}_A$, should not depend on the acceptance. This is explicitly the case in equilibrium and we have verified that this remains approximately the case in all of our simulations.

We present our final results for the normalized fluctuation measure for protons and pions, $\tilde{\omega}_p$ and $\tilde{\omega}_\pi$, in Figs. 13 and 14. These results demonstrate that for trajectories passing closer to the critical point (i.e., for trajectories with larger $\xi_{\max}$) the magnitude of fluctuations is larger, as we have already seen in Fig. 7 for the Bjorken expansion scenario. Again as in the Bjorken scenario, the magnitude of the effect depends on the rate of the diffusive relaxation of the fluctuations controlled by parameter D_0. The conservation laws (i.e., "memory") lead to significant suppression of the magnitude of fluctuations compared to the prediction based on the assumption that fluctuations

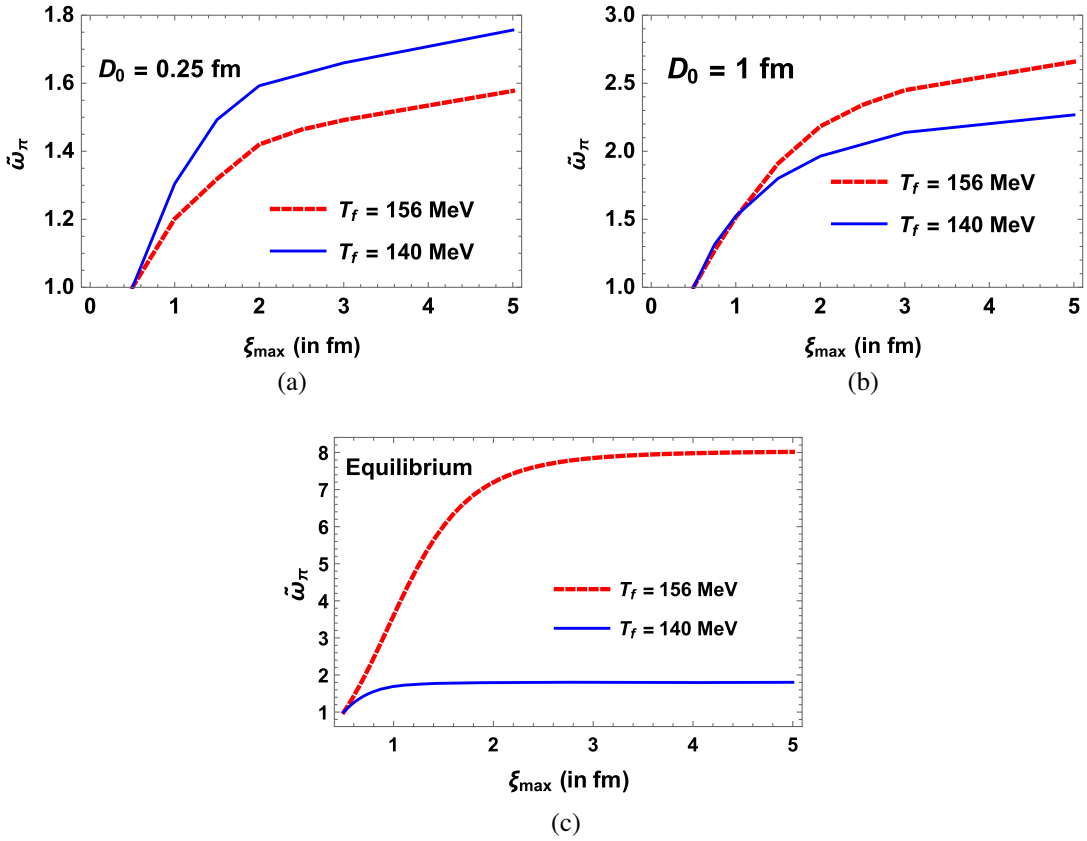

FIG. 14. Normalized measure of the fluctuations in pion multiplicity, $\tilde{\omega}_\pi = \frac{\omega_\pi}{\omega_\pi^{\rm nc}}$, as a function of the maximum equilibrium correlation length along the system trajectory, which is to say as a function of how closely the trajectory passes the critical point. As $D_0 \to \infty$, the $\tilde{\omega}_\pi$'s approach their equilibrium values shown in panel (c). The definition of the normalized measure of fluctuations $\tilde{\omega}$ is such that it is species-independent in equilibrium, meaning that panel (c) here is identical to panel (c) in Fig. 13.

have enough time to equilibrate. [The equilibrium predictions are shown in Figs. 13(c) and 14(c).] The smaller the value of the diffusion parameter D_0, i.e., the slower is the diffusion, the stronger is the suppression.

It is also interesting to compare the magnitude of fluctuations for the same value D_0 and $\xi_{\rm max}$, but for two different freeze-out temperatures. Naturally, the equilibrium assumption leads to a prediction of larger fluctuations at higher freeze-out temperature, since the higher temperature is closer to the critical point. However, nonequilibrium effects not only suppress the magnitude of the fluctuations relative to the equilibrium prediction but also introduce memory effects that substantially reduce the decrease in the magnitude of the fluctuations that occurs between $T = 156$ MeV and the lower freeze-out temperature $T_f = 140$ MeV. This makes the fluctuations obtained upon assuming a freeze-out temperature of $T_f = 140$ MeV much more similar in magnitude to those that would be obtained if $T_f = 156$ MeV than is the case in equilibrium. So much so, in fact, that, depending on the choice of the parameters such as D_0, it is even possible to find larger fluctuations at $T_f = 140$ MeV than would have been obtained at the higher freeze-out temperature $T_f = 156$ MeV, see Figs. 13(a) and 14(a). This effect arises because, as we have already discussed, the fluctuations continue to grow even after the system has passed the critical point, as long as their value is below the equilibrium, as can be seen in Fig. 10. This effect is not seen in the Bjorken scenario in Sec. III because the drop of the temperature during the one-dimensional longitudinal expansion there is much slower than in our calculations in this section which include radial expansion in addition. As a result, in the Bjorken scenario the freeze-out temperatures are reached at somewhat later times, after the nonequilibrium fluctuations have began to decrease. For the same reason, in our more realistic calculations in this section this effect disappears for larger values of D_0 which yields faster relaxation of fluctuations toward equilibrium, see Figs. 13(b) and 14(b).

V. SUMMARY AND OUTLOOK

In this work, we have introduced a novel approach which connects hydrodynamic fluctuations, which fall out of equilibrium during the hydrodynamic stage of the expansion and cooling of the droplets of QGP produced in heavy ion collisions, to subsequent fluctuations of particle

multiplicities, observable in experiments. In this approach, we treat the hydrodynamic fluctuations in the Hydro+ formalism [18], focusing on the critical, which is to say the most singular as well as the slowest—and thus the most out-of-equilibrium—modes of fluctuations near the critical point. On the kinetic, or particle, side of the freeze-out, such fluctuations are matched by introducing a new critical scalar field σ which couples to observable particles. One can understand this field as an effective critical field—a collective phenomenon in the hadron gas—a precursor of the critical point. It has the same quantum numbers as the σ meson, meaning that its couplings to other hadrons, including protons, are such that fluctuations in σ correspond to fluctuations in the masses of other hadrons, including protons. In prior estimates of the observable consequences of critical fluctuations, the σ field and in particular its fluctuations were assumed to stay in equilibrium near the critical point for lack, at the time, of an approach to describing its nonequilibrium evolution. In this paper, we connect the fluctuations of this field, and consequent observable fluctuations in particle multiplicities, to the Hydro+ variable $\phi_{\boldsymbol{Q}}$, which describes the nonequilibrium evolution of fluctuations in the earlier hydrodynamic stage of the collision.

Our approach generalizes the well-known and well-tested Cooper-Frye freeze-out [44], which translates hydrodynamic degrees of freedom (but not their fluctuations) into particle distributions. The Cooper-Frye procedure only specifies event-averaged single-particle quantities (multiplicities and spectra of each hadron species) and as such is not sufficient to describe the freeze-out of *fluctuations* or *correlations*. Our more general freeze-out procedure allows us to perform such a translation, or matching, of Hydro+ (hydrodynamic and fluctuation) degrees of freedom to particle multiplicities and their fluctuations.

We demonstrate our generalized freeze-out procedure in practice by freezing out a simplified case (the Hydro+ description of boost-invariant Bjorken expansion with no transverse expansion) where the calculations can largely be pushed through analytically and that yields valuable intuition as well as a numerical Hydro+ simulation of a more realistic scenario with boost invariance and azimuthal symmetry that incorporates transverse radial expansion, similar to the one considered in Ref. [14]. In both examples, we observed a significant suppression of the out-of-equilibrium fluctuations relative to what their values would have been in equilibrium for reasonable values of the parameters we considered. In addition, we also noted that while the *equilibrium* fluctuations sensitively depend on how soon, i.e., how far below the critical temperature, the freeze-out occurs, this sensitivity is almost eliminated by nonequilibrium ("memory") effects, see Figs. 7, 13, and 14.

The Hydro+ variable $\phi_{\boldsymbol{Q}}$ describes the magnitude of the fluctuations at different wave vectors $\boldsymbol{Q}$. We observe [and, in the case of the Bjorken scenario, can describe analytically as in Eq. (58)] that the characteristic value of the wavenumber Q whose $\phi_{\boldsymbol{Q}}$'s control the magnitude of the multiplicities after freeze-out is determined by multiple factors including the scale of the inhomogeneity of the expanding fluid (the Bjorken time τ in the Bjorken scenario), the radial flow, the typical thermal velocity spread of the produced particles, as well as the acceptance window in rapidity if this acceptance window is larger than the typical thermal spread in rapidity. This characteristic Q is small compared to microscopic scales as it is typically of order $1/\tau_f$ [see Eq. (58)]. Since the fluctuations at small Q are suppressed by conservation laws (another aspect of the out-of-equilibrium dynamics that is in a sense also a "memory" effect), the smallness of the characteristic Q relevant for the freeze-out contributes to the suppression of the fluctuations relative to the equilibrium values.

Our study focused on Gaussian measures of fluctuations. The higher, non-Gaussian, cumulants are more sensitive to the proximity of the critical point [8,10]. It is, therefore, important to generalize our freeze-out procedure to higher-order cumulants. This can be done using Eq. (28) and we leave implementation and the analysis of the results to future work. While we demonstrated the application of our procedure to the variance of particle multiplicities, it will also be straightforward to generalize to the cross-correlation of different particle species, as was done in Ref. [10] for equilibrium fluctuations. We expect the conclusion from that work that cumulants involving protons are most sensitive to critical fluctuations to persist, but we leave an investigation of how best to combine measurements of different (cross-)correlations so as to optimize the sensitivity to critical fluctuations while reducing dilution of their effects by backgrounds to future work.

We have focused on the *dependence* of the observable fluctuations on the proximity of the critical point, either by varying $\xi_{\max}$, which corresponds to varying freeze-out μ_B via changing collision energy $\sqrt{s}$ (see Fig. 1), or by varying the freeze-out temperature (for the same trajectory). We also studied the dependence on the (thus far unknown) value of the diffusion parameter D_0. In order to illustrate these dependencies, we chose to present our results using normalized variables which did not depend on the *absolute* magnitude of the effect. In order to predict the absolute magnitude one would have to know the equation of state, i.e., the parameter Z in Eq. (22) which determines the absolute strength of the singularity. Also, one would have to determine the couplings g_A of hadrons to the critical collective field σ. These couplings are, of course, also related to the equation of state and it would be interesting to make this relation more explicit. We leave this to future work. For the purpose of using our results to make crude estimates, one could take $Z \sim 1/T_c^2$ and follow Ref. [10] and choose $g_p \sim 7$ and $g_\pi \sim 2$.

It would be also interesting to consider going beyond the leading critical behavior of fluctuations to take into account less singular critical contributions and modes

which are not critical, including fluctuations of pressure and flow velocity. Extending our work in this way would be necessary in order to attempt to develop a fluctuation freeze-out procedure that could be applied away from the critical point as well as near it, as in our paper.

It is also important to realize that we considered fluctuations and freeze-out on the crossover side of the critical point (see Fig. 1). It would also be interesting and important to understand what happens on the other side, where the first-order phase transition occurs. The challenge in this domain begins already at the level of hydrodynamics and is beyond the scope of this paper.

Although, as we have detailed in this section, there is a scope for improvement and generalization of the freeze-out procedure that we have introduced and explored in this paper, we believe that the procedure can already be integrated into the full numerical simulation of heavy-ion collisions relevant for the BES program aimed at the search for the QCD critical point. With first results from high-statistics BES data taken at RHIC in 2019-2021 anticipated soon, this represents a high priority next step.

ACKNOWLEDGMENTS

We gratefully acknowledge the contributions of Ryan Weller, who collaborated with us on this research project in its early stages. We acknowledge helpful conversations with Travis Dore, Lipei Du, Jamie Karthein, Gregory Ridgway and Chun Shen. This work was supported by the U.S. Department of Energy, Office of Science, Office of Nuclear Physics, within the framework of the Beam Energy Scan Theory (BEST) Topical Collaboration and Grants No. DE-SC0011090 and No. DE-FG0201ER41195. Y. Y. acknowledges support from the Strategic Priority Research Program of the Chinese Academy of Sciences, Grant No. XDB34000000.

APPENDIX A: EQUATION OF STATE USED IN THE HYDRODYNAMICAL EVOLUTION

The equation of state that we have used in the analytical calculations of Sec. III, done within a Bjorken scenario, as well as in the numerical Hydro+ simulations for a semi-realistic scenario done in Sec. IV, is taken from Ref. [14]. We describe this equation of state briefly in this Appendix. An aspect of the physics that the Hydro+ formalism is well suited to describe is the way in which the out-of-equilibrium fluctuations of the slow modes modify the equation of state [18]. However, it has been observed in Refs. [14,30] that these backreaction effects are smaller than 1% in most cases. For this reason, throughout the present work we neglect the feedback of Hydro+ modes on the equation of state. That is, in the notation of Refs. [14,18,30] we approximate the Hydro+ equation of state $p_+(\varepsilon)$ by the standard pressure $p(\varepsilon)$ given by

$$p = \frac{s}{\beta} - \varepsilon \tag{A1}$$

where ε is the energy density, β is the inverse temperature, and where the entropy density s is given as a function of the local temperature by

$$s(T) = \int_0^T dT' \frac{c_V(T')}{T'} \tag{A2}$$

with $c_V(T)$ being the specific heat capacity at fixed volume. In Ref. [14], the equation of state is specified close to and away from a critical temperature T_c by choosing

$$c_V(T) = \begin{cases} c_V^{\text{no C.P}}(T) & T \le T_L \text{ or } T \ge T_H \\ c_V^{\text{crit}}(T) + \sum_{n=0}^{5} c_n \left(\frac{T-T_c}{\Delta T}\right)^n & T_L < T < T_H \end{cases} \tag{A3}$$

with $(T_L, T_H) = (T_c - \Delta T, T_c + \Delta T)$ and where ΔT, which parametrizes the width of the critical region, is the same parameter that arises in Eq. (11). Here as there, we take $\Delta T = T_c/5$. Following Ref. [14], we take $c_V^{\text{crit}}(T)$, the critical part of c_V that shows the leading singular behavior near the critical point, to have the form

$$c_V^{\text{crit}}(T) \equiv \frac{1}{2}\frac{1}{\xi_0^3}\frac{\xi(T)}{\xi_0}, \tag{A4}$$

where the temperature dependence of the correlation length of critical fluctuations, $\xi(T)$, needs to be specified. Following Ref. [14], we do so as in Eq. (11). The prefactor $1/2$ in Eq. (A4) is a nonuniversal constant whose value depends on the mapping between the equation of state of the 3D Ising model and the equation of state of QCD, whose critical point is in the 3D Ising universality class. We have used a value that is reasonable for $\Delta T = T_c/5$; see the argument in Ref. [14]. Continuing to follow Ref. [14], away from the critical point we choose the form of the specific heat capacity $c_V^{\text{no C.P}}(T)$ as follows:

$$\frac{c_V^{\text{no C.P}}(T)}{T^3} \equiv \left[\frac{a_H + a_L}{2} + \frac{a_H - a_L}{2}\tanh\frac{T - T_{\text{crossover}}}{\Delta T_{\text{crossover}}}\right] \tag{A5}$$

with

$$a_L = 0.1\, a_{\text{QGP}}, \qquad a_H = 0.8\, a_{\text{QGP}}, \quad \text{and}$$
$$a_{\text{QGP}} \equiv \frac{4\pi^2(N_c^2 - 1) + 21\pi^2 N_f}{15}, \tag{A6}$$

where $N_c = 3$ and $N_f = 3$ are the number of flavors and colors, respectively, and with

$$T_{\text{crossover}} = T_c, \qquad \Delta T_{\text{crossover}} = 0.6T_c. \tag{A7}$$

The specification of the equation of state is completed by choosing the six constant coefficients c_n that appear in Eq. (A3) so as to enforce that $c_V(T)/T^3$ and its first two derivatives are continuous at $T = T_L$ and at $T = T_H$.

APPENDIX B: ANALYTICAL CALCULATIONS IN A BJORKEN SCENARIO

In this Appendix, we derive an explicit expression for the numerator of $C_A(\Delta y)$ defined in Eq. (56), namely $\langle \delta\frac{dN_A}{dy_+}\delta\frac{dN_A}{dy_-}\rangle_\sigma$, in the Bjorken symmetric background described in Sec. III. We shall begin from the somewhat formal expression for $\langle \delta N_A^2\rangle_\sigma$ that we obtained in Eq. (50), develop an explicit expression for this measure of fluctuations in the Bjorken background, and then see that we can obtain the explicit expression (57) for the rapidity correlator $\langle \delta\frac{dN_A}{dy_+}\delta\frac{dN_A}{dy_-}\rangle_\sigma$ essentially by inspection of the explicit form of $\langle \delta N_A^2\rangle_\sigma$.

In the second half of the Appendix, as a bonus we shall use the analytic control that we have over the calculation of $\langle \delta N_A^2\rangle_\sigma$ to show that the low-Q modes of $\phi_{\boldsymbol{Q}}$ make the dominant contribution to this observable.

We begin by noting that in the Bjorken scenario we have the following expressions for x and $\Delta x_\perp$ at $\tau = \tau_f$:

$$x = \tau_f \cosh\Delta\eta\hat{\tau} + x_T \tag{B1a}$$

$$\Delta x_\perp = \Delta x = 2\tau_f \sinh\frac{\Delta\eta}{2}\hat{\eta} + \Delta x_T. \tag{B1b}$$

Equations (B1) are exact for two points x_+ and x_- on the freeze-out hypersurface and can be obtained by substituting $u^\tau = 1$, $u^r = 0$, $\tau = \tau_f$ and $\Delta\tau = 0$ in Eqs. (46). We have used x_T and Δx_T to denote the transverse parts of x and $\Delta x_\perp$, namely their projections onto the plane spanned by $\hat{r}$ and $\hat{\varphi}$. Note that because points on the freeze-out surface, including x_+ and x_-, all have the same τ in the Bjorken scenario, $\Delta x_\perp = \Delta x$ in this setting and Eq. (50) need not be corrected as described around Fig. 3.

Next, we note that the $\tilde{\phi}$ that arises in the expression (50) that we wish to evaluate is the inverse Wigner transform of $\phi_{\mathbf{Q}}$, see Eq. (21). In the Bjorken scenario, this transform takes the form

$$\tilde{\phi}(x,\Delta\mathbf{x}) = \int \frac{d\mathbf{Q}_\perp dQ_\eta}{(2\pi)^3} e^{i2Q_\eta\tau_f\sinh\frac{\Delta\eta}{2} + i\mathbf{x}_\perp\cdot\Delta\mathbf{x}_T}\phi_{\mathbf{Q}}(\tau_f\cosh\Delta\eta) \tag{B2}$$

where $Q_\eta \equiv Q\cdot\hat{\eta}$ and $\mathbf{Q}_\perp \equiv \mathbf{Q} - Q_\eta\hat{\eta}$. Note that since points on the freeze-out hypersurface all have the same τ in the Bjorken scenario, the expression for the two-point correlator of σ between two points on the freeze-out hypersurface given by Eq. (31) does not receive the correction described following that equation. Note that $\phi_{\mathbf{Q}}$ that enters Eq. (B2) is obtained by solving Eq. (53), as discussed in Sec. III. Later in this Appendix, we shall need the formal solution to Eq. (53) that satisfies the initial conditions (54); it is given by

$$\phi_{\mathbf{Q}}(\tau) = \bar{\phi}_{\mathbf{Q}}(T_i)e^{-\int_{\tau_i}^{\tau}\Gamma(Q\xi(\tau'))d\tau'} + \int_{\tau_i}^{\tau} e^{-\int_{\tau''}^{\tau}\Gamma(Q\xi(\tau'))d\tau'}\Gamma(Q\xi(\tau''))\bar{\phi}_{\mathbf{Q}}(T(\tau''))d\tau'' \tag{B3}$$

The functional form for the evolution of temperature $T(\tau)$, which also determines $\xi(\tau)$ through Eq. (11), can be obtained from the condition

$$\tau s(T(\tau)) = \tau_i s(T(\tau_i)) \tag{B4}$$

that follows from the isentropic nature and Bjorken symmetry of the flow and that must be satisfied for all $\tau_i < \tau < \tau_f$. And, we employ the equation of state $s(T)$ from Ref. [14] that we describe briefly in Appendix A.

With these preliminaries in place, we now substitute Eq. (B2) into Eq. (50) and integrate over $d\mathbf{x}_\mathbf{T}$, $d\Delta\mathbf{x}_\mathbf{T}$ and $d\mathbf{Q}_\perp$, obtaining

$$\langle \delta N_A^2\rangle_\sigma = g_A^2 A_\perp \tau_f^2 \int_{-\infty}^{\infty} d\eta \int_{-\infty}^{\infty} d\Delta\eta I_A(\eta_+,\eta_-) \times \int \frac{dQ_\eta}{2\pi} e^{i2Q_\eta\tau_f\sinh\frac{\Delta\eta}{2}}\phi_{\mathbf{Q}_\parallel}(\tau_f\cosh\Delta\eta), \tag{B5}$$

where we have defined $\mathbf{Q}_\parallel \equiv Q_\eta\hat{\eta}$, where $A_\perp$ is the transverse area in the plane spanned by $\hat{r}$ and $\hat{\varphi}$, and where we have defined

$$I_A(\eta_+,\eta_-) \equiv n(\eta_+)\cdot J_A(\eta_+)n(\eta_-)\cdot J_A(\eta_-). \tag{B6}$$

Upon explicit evaluation, this function is given by

$$I_A(\eta_+,\eta_-) = \int_{y_{\min}}^{y_{\max}} dy_+ \int_{y_{\min}}^{y_{\max}} dy_- F_A(y_+ - \eta_+)F_A(y_- - \eta_-) \tag{B7}$$

where

$$F_A(y_\pm - \eta_\pm) \equiv \frac{d_A m_A}{T_f}\frac{dy}{2\pi}\int_{m_{T,\min}}^{m_{T,\max}} \frac{m_T dm_T}{2\pi} e^{-\frac{m_T\cosh(y_\pm - \eta_\pm)}{T_f}}. \tag{B8}$$

Upon specifying $m_{T,\min} = m_A$ and choosing $m_{T,\max} = \infty$ and $y_{\min} = -y_{\max}$, F_A is given by

$$F_A(x) = d_A \frac{m_A}{T_f} \int_{m_A}^{\infty} \frac{m_T dm_T}{(2\pi)^2} e^{-\frac{m_T \cosh x}{T_f}} \tag{B9a}$$

$$= d_A m_A (2\pi)^{-2} \mathrm{sech}^2 x (m_A \cosh x + T_f) e^{-\frac{m_A \cosh x}{T_f}}. \tag{B9b}$$

Using the expressions above, Eq. (B6) can be evaluated directly, numerically. However, to elucidate its main features we ignore the subleading corrections due to the curvature of the freeze-out hypersurface and assume that $m_A \gg T$, in both cases as discussed in Sec. II C. This allows us to make the following approximations:

$$\phi_{\mathbf{Q}_\parallel}(\tau_f \cosh \Delta\eta) \approx \phi_{\mathbf{Q}_\parallel}(\tau_f) \tag{B10a}$$

$$F_A(\eta_\pm) \approx d_A m_A^2 (2\pi)^{-2} \mathrm{sech}\eta e^{-\frac{m_A}{T_f}[\cosh\eta \pm \frac{\sinh\eta}{2}\Delta\eta + \frac{\cosh\eta}{8}\Delta\eta^2]} \tag{B10b}$$

The assumption $m_A \gg T$ has allowed us to simplify Eq. (B10b) by expanding only the exponential term in F_A as a function of $\Delta\eta$ and not its prefactor. We have verified by explicit calculation that this assumption is well justified for protons. With the above simplifications, after defining $\Delta y \equiv y_+ - y_-$ and redefining the variables η and $\Delta\eta$ according to $\eta \to \eta - (y_+ + y_-)/2$ and $\Delta\eta \to \Delta\eta - \Delta y$, Eq. (B6) becomes

$$\langle \delta N_A^2 \rangle_\sigma \approx g_A^2 T_f A_\perp \tau_f^2 \int_{-\infty}^{\infty} d\eta \int_{-\infty}^{\infty} d\Delta\eta F_A(\eta+) F_A(\eta_-) \times \int_{-y_{\max}}^{y_{\max}} dy_+ \int_{-y_{\max}}^{y_{\max}} dy_- \int \frac{dQ_\eta}{2\pi} e^{iQ_\eta \tau_f (\Delta\eta + \Delta y)} \phi_{\mathbf{Q}_\parallel}(\tau_f). \tag{B11}$$

This explicit expression for the observable measure of the fluctuations $\langle \delta N_A^2 \rangle_\sigma$ is the first main result of this Appendix.

Upon inspection of the result (B11), we see that the two point rapidity space correlator occurring in $C_A(\Delta y)$ is given by

$$\left\langle \delta \frac{dN_A}{dy_+} \delta \frac{dN_A}{dy_-} \right\rangle_\sigma \approx g_A^2 T_f A_\perp \tau_f^2 \int_{-\infty}^{\infty} d\eta \int_{-\infty}^{\infty} d\Delta\eta F_A(\eta+) F_A(\eta_-) \times \int \frac{dQ_\eta}{2\pi} e^{iQ_\eta \tau_f (\Delta\eta + \Delta y)} \phi_{\mathbf{Q}_\parallel}(\tau_f) \tag{B12}$$

$$\approx \frac{1}{8\pi^{7/2}} g_A^2 d_A^2 Z^{-1} m_A^{7/2} T_f^{1/2} A_\perp \tau_f^2 \int d\eta \mathrm{sech}^{5/2}\eta e^{-\frac{2m_A \cosh\eta}{T_f}} \times \int \frac{dQ_\eta}{2\pi} e^{iQ_\eta \tau_f \Delta y} e^{-\frac{Q_\eta^2 \tau_f^2 T_f}{m_A \cosh\eta}} \phi_{\mathbf{Q}_\parallel}(\tau_f). \tag{B13}$$

Eq. (B13), our second main result of this Appendix, is reproduced in Sec. III as Eq. (57) and its implications are discussed there.

In the remainder of this Appendix, we shall demonstrate that the low Q modes of $\phi_{\mathbf{Q}}$ contribute the most to the variance of particle multiplicities, $\langle \delta N_A^2 \rangle_\sigma$. We shall expand

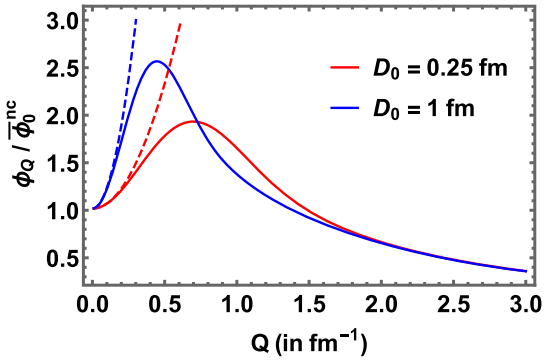

(a) ϕ at freeze-out

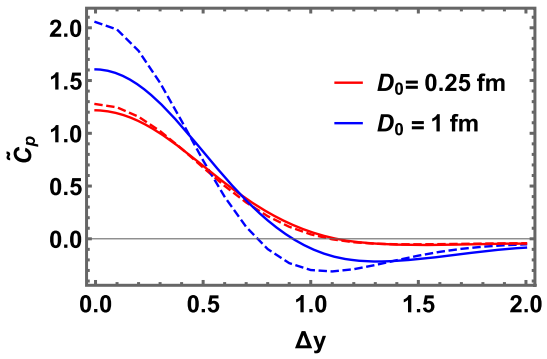

(b) $\tilde{C}(\Delta y)$ for protons

FIG. 15. Panel (a): Normalized ϕ as a function of Q evolved according to model H dynamics with two values of D_0, plotted at freeze-out $\tau = \tau_f$, corresponding to an equilibrium temperature of $T_f(\tau_f) = 140$ MeV. The solid and dashed curves were obtained from the full solution (B3) for $\phi_{\mathbf{Q}}$ and its truncated polynomial expansion (B14) respectively. Panel (b): Normalized fluctuation measure observable (rapidity space correlator) for protons $\tilde{C}_p(\Delta y)$ obtained with the full form (solid) and truncated form (dashed) of $\phi_{\mathbf{Q}}$. The qualitative and even semiquantitative agreement between the same colored curves in the right plot indicates that the low-Q modes contribute significantly to the variance of particle multiplicities. In obtaining these plots, $\xi_{\max}$ was set to 3 fm and the fluctuations at $\tau_i = 1$ fm were initialized to their equilibrium value at $\tau = \tau_i = 1$ fm with $T_i(\tau_i) = 235$ MeV.

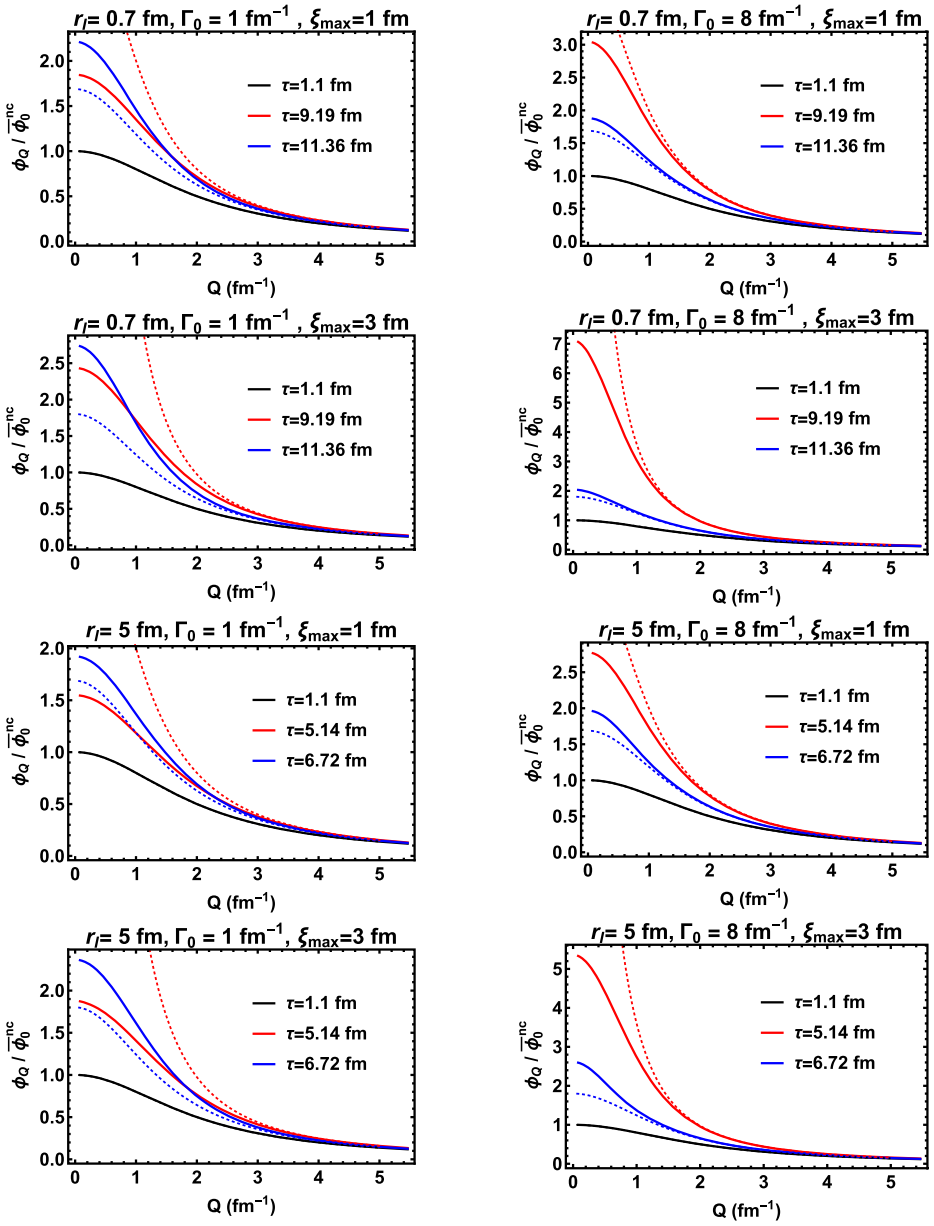

FIG. 16. Hydro+ fluctuation measure $\phi_{\mathbf{Q}}$ evolved according to model A dynamics along two hydrodynamic flow lines passing through $r = r_i$ at initial time $\tau = \tau_i$, with $r_i = 0.7$ fm (top four panels) and 5 fm (bottom four panels). Plots in the left (right) column are for $\Gamma_0 = 1$ fm^{-1} ($\Gamma_0 = 8$ fm^{-1}), with $\xi_{\max} = 1$ fm and $\xi_{\max} = 3$ fm in alternating rows. The solid (and dashed) curves are the ϕ_Q (and $\bar{\phi}_Q$), normalized to the zero mode of the noncritical fluctuations. The black, red and blue curves correspond to $\phi_{\mathbf{Q}}$'s at the initial time τ_i and at the times when the equilibrium temperature reaches 160 MeV and 140 MeV respectively.

$\phi_{\mathbf{Q}}$, given by Eq. (B3), in powers of $\mathbf{Q}$ to $\mathcal{O}(\mathbf{Q}^2)$ and compare the result for $\langle \delta N_A^2 \rangle_\sigma$ that we obtain starting from this expansion to the result that we obtain starting from the full form of $\phi_{\mathbf{Q}}$. We denote the polynomial expansion for $\phi_{\mathbf{Q}}$ to quadratic order by

$$\phi_{\mathbf{Q}} \approx \phi^{(0)} + \phi^{(2)} Q^2 \tag{B14}$$

where

$$\phi^{(0)} = Z T_f \xi^2(T_i) \tag{B15a}$$

$$\phi^{(2)} = -Z T_f \xi^4(T_i) + 2 D_0 \xi_0 Z T_f \int_{\tau_i}^{\tau_f} d\tau \left(\xi(T(\tau)) - \frac{\xi^2(T_i)}{\xi(T(\tau))} \right). \tag{B15b}$$

The expression (B14) is a good approximation to $\phi_{\mathbf{Q}}$ for its low-Q modes, as we illustrate in Fig. 15(a).

Upon making the low-Q approximation and working to order Q^2 as in Eq. (B14), we can perform the Q_η integral in Eq. (B13), obtaining

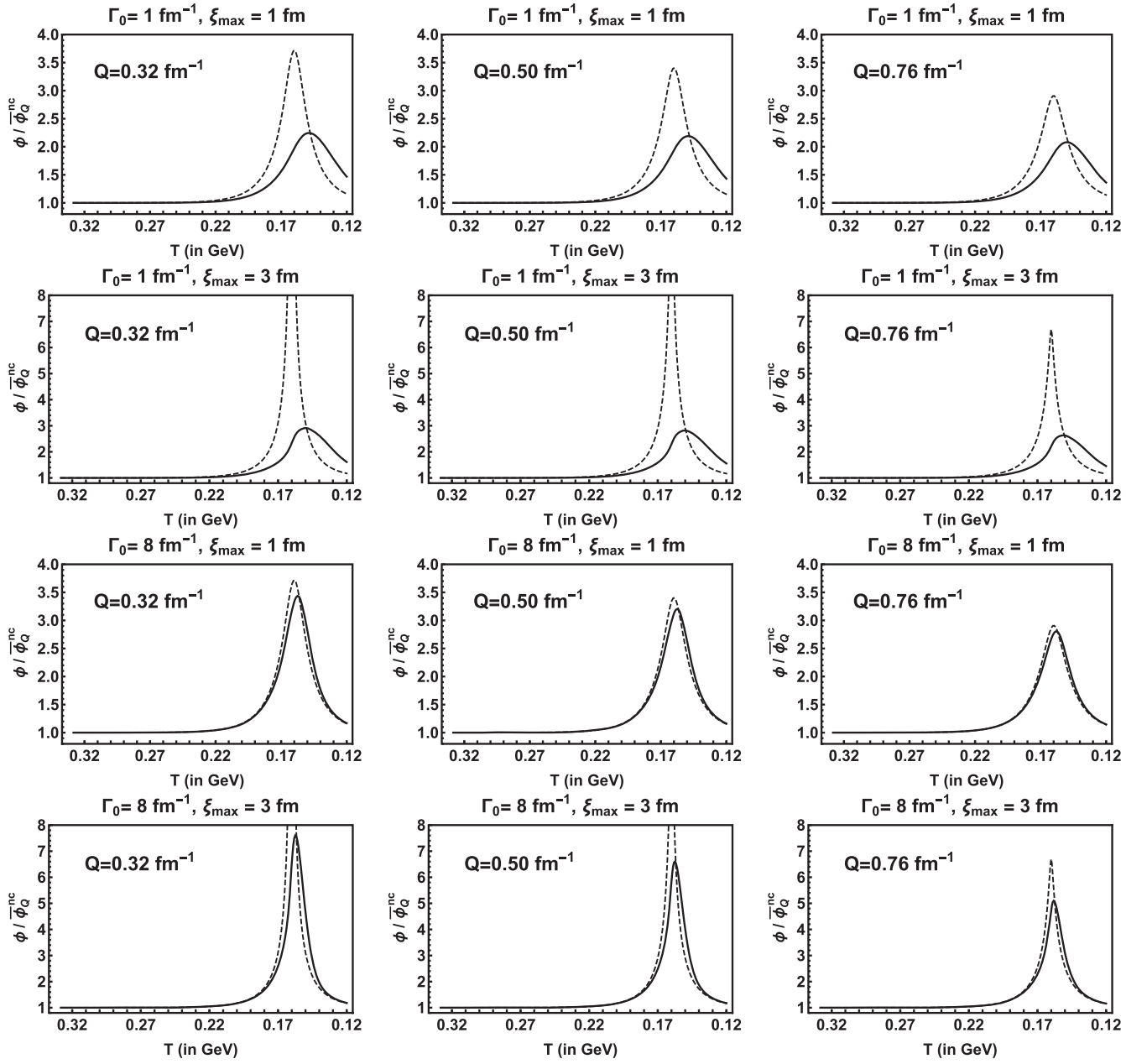

FIG. 17. The values of ϕ_Q (suitably normalized) for three representative values of Q (same for each column), and for two values Γ_0 (same in top and bottom six panels) and $\xi_{\max}$ (same in alternating rows) as in Fig. 16. The values of ϕ_Q are taken along a fluid cell trajectory and plotted as a function of temperature, which is a monotonous function of time τ along the trajectory. The trajectory chosen for these plots begins at $r_i = r(\tau_i) = 1.8$ fm. The dashed and solid curves represent the equilibrium $\bar{\phi}_Q$ and nonequilibrium ϕ_Q, respectively.

$$\left\langle \delta\frac{dN_A}{dy_+}\delta\frac{dN_A}{dy_-}\right\rangle_\sigma \approx \frac{g_A^2 d_A^2 A_\perp \tau_f Z^{-1} m_A^4}{(2\pi)^4}\int \frac{d\eta}{\cosh^2\eta} e^{-\frac{2m_A\cosh\eta}{T_f}(1+\frac{\Delta y^2}{8})}\left[\phi^{(0)} + \frac{2T_f m_A\cosh\eta - \Delta y^2 m_A^2\cosh^2\eta}{4\tau_f^2 T_f^2}\phi^{(2)}\right]. \tag{B16}$$

In Fig. 15(b), we compare $\tilde{C}_p(\Delta y)$ (defined via Eqs. (56), (59), and (60) obtained from $\langle \delta\frac{dN_A}{dy_+}\delta\frac{dN_A}{dy_-}\rangle_\sigma$ computed without making a low-Q approximation, namely Eq. (B13), which is plotted as the solid curves in Fig. 15(b), to that computed upon working only to order Q^2, namely Eq. (B16), which is plotted as the dashed curves in Fig. 15(b). The qualitative, even semiquantitative, agreement between them indicates that the low-Q modes contribute significantly to the variance of particle multiplicities.

APPENDIX C: CONTRASTING WITH MODEL A EVOLUTION

In this Appendix we repeat the calculations of Sec. IV in a scenario in which the hydrodynamic background is the same (and hence also the same as in Ref. [14]) but in which the dynamical evolution of the fluctuations differs. In Sec. IV we take conservation laws into account, following model H dynamics. Here, in contrast, we shall consider the case where the fluctuating slow mode is not a conserved quantity, meaning that the appropriate dynamics for the relaxation of the two-point function is that of model A in the classification of Halperin and Hohenberg [54], with the relaxation rate given by Eq. (10), which we repeat here:

$$\Gamma(\boldsymbol{Q}) = \Gamma_0 \frac{\xi_0^2}{\xi^2}(1 + (Q\xi)^2), \qquad \text{(model A)}. \quad \text{(C1)}$$

We have performed simulations with $\Gamma_0 = 1$ fm^{-1} and 8 fm^{-1}, which correspond to $\Gamma_0\xi_0^2 = 0.25$ fm and 2 fm, respectively. Comparing the "shapes" of all the results plotted in this Appendix to those in the analogous Figures in Sec. IV provides us with another way of seeing the impact of conservation laws on the results from Sec. IV. The main difference between model A and model H evolution arises from the qualitatively different relaxation rate for the low Q modes, $Q\xi \ll 1$, which goes as $\Gamma_0\xi_0^2/\xi^2$ in model A and as $(D_0\xi_0/\xi)Q^2$ in model H, with the Q^2-suppression being a manifestation of conservation. A second motivation for this Appendix is that, because model A dynamics is simpler to implement, in their pioneering calculation the authors of Ref. [14] used model A dynamics, meaning that in this Appendix we shall be freezing out the calculations of Ref. [14], turning these Hydro+ simulations into particle multiplicity fluctuations.

1. Evolution of ϕ_Q

In Fig. 16, which can be compared to the analogous model H results shown in Fig. 9, we illustrate the model A dynamics of ϕ_Q for fluid cells following two different hydrodynamic flow lines, with two choices of Γ_0 and two choices of $\xi_{\max}$. As in Sec. IV, varying $\xi_{\max}$ corresponds to varying how close the cooling trajectory of the fluid cell comes to the critical point on the phase diagram.

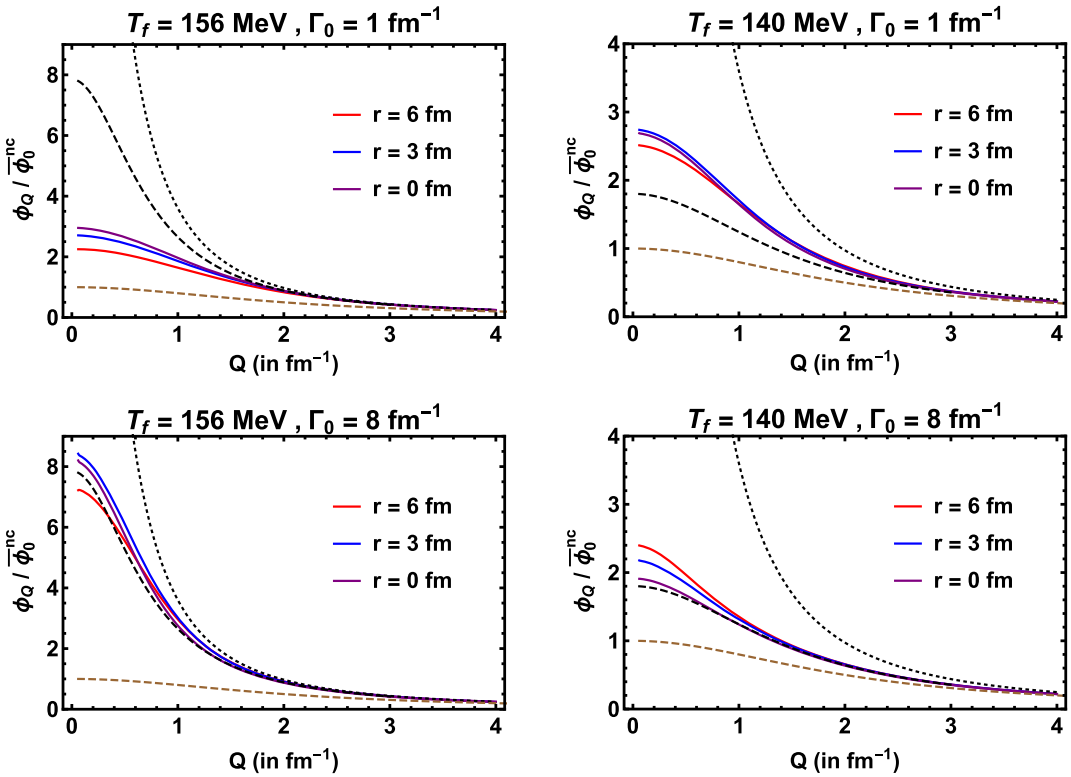

FIG. 18. The Hydro+ variable ϕ_Q (normalized to its value at $Q = 0$ away from the critical point, where $\xi = \xi_0$) at freeze-out evolved with $\Gamma_0 = 1$ fm^{-1} (upper panels) and 8 fm^{-1} (lower panels) and with $\xi_{\max} = 3$ fm. The left (right) panels show results for evolution until the decreasing temperature has reached a higher (lower) freeze-out temperature. The blue, red and purple curves show the values of ϕ_Q at different points on the freeze-out hypersurface, characterized by the radial coordinate r. The black dashed and dotted curves are the equilibrium curves at $T = T_f$ and $T = T_c$ respectively. The dashed brown curve is the (noncritical) equilibrium curve corresponding to $\xi = \xi_0$.

The central qualitative difference between the model A results in Fig. 16 and the model H results in Fig. 9 is that in model H $\phi_{\mathbf{Q}}$ at $Q = 0$ is unchanging in time, because of conservation, which means that as critical fluctuations develop we see that in Fig. 9 $\phi_{\mathbf{Q}}$ takes on a shape in which it first rises as a function of increasing Q and then falls whereas in the model A dynamics of this Appendix the maximum value of $\phi_{\mathbf{Q}}$ is found at $Q = 0$, and this value is time dependent. In model A, here, as in model H in Fig. 9, the fluctuations $\phi_{\mathbf{Q}}$ fall out of equilibrium, lagging behind the equilibrium fluctuations $\bar{\phi}_{\mathbf{Q}}$ as the latter change with time.

In Fig. 17, which can be compared to the analogous model H results shown in Fig. 10, for all three representative Q modes that are plotted we notice the $\phi_{\mathbf{Q}}$'s lagging behind their respective $\bar{\phi}_{\mathbf{Q}}$s, with the degree to which they fall out of equilibrium greater for smaller Γ_0, meaning slower relaxation toward equilibrium. For the values of Γ_0 that we have considered in Fig. 17, we can see that fluctuations do depend on whether we choose a freeze-out temperature of 156 MeV or 140 MeV. As we also observed in Fig. 10, $\phi_{\mathbf{Q}}$ has an inflection point at $T = T_c$ where the relaxation rate takes its minimum value and the growth of $\phi_{\mathbf{Q}}$ stops when $\phi_{\mathbf{Q}}$ equals the instantaneous $\bar{\phi}_{\mathbf{Q}}$.

2. Fluctuations on the freeze-out surface

In Fig. 18, which can be compared to Fig. 11, suitably normalized plots of $\phi_{\boldsymbol{Q}}$ are shown for three points on the freeze-out hypersurface, characterized by radial coordinate $r = 0$, 3 and 6 fm, for two choices of freeze-out temperature T_f and two values of the parameter Γ_0. Most of the discussion of Fig. 11 in Sec. IV applies here also, with the one significant difference being that here the $Q = 0$ modes are not "stuck" at their initial values.

As in Fig. 12, in Fig. 19 we have computed $\tilde{\phi}(\Delta \boldsymbol{x}_\perp)$, the inverse Fourier transform of $\phi_{\boldsymbol{Q}}$ defined in Eq. (32), and plotted $\Delta x^2 \tilde{\phi}(\Delta \boldsymbol{x}_\perp)$ as a function of the spatial separation Δx between the two points in the correlator $\langle \delta\hat{s}(x_+)\delta\hat{s}(x_-)\rangle$. As in the model H evolution of Fig. 12, the small Δx (large Q) behavior of the

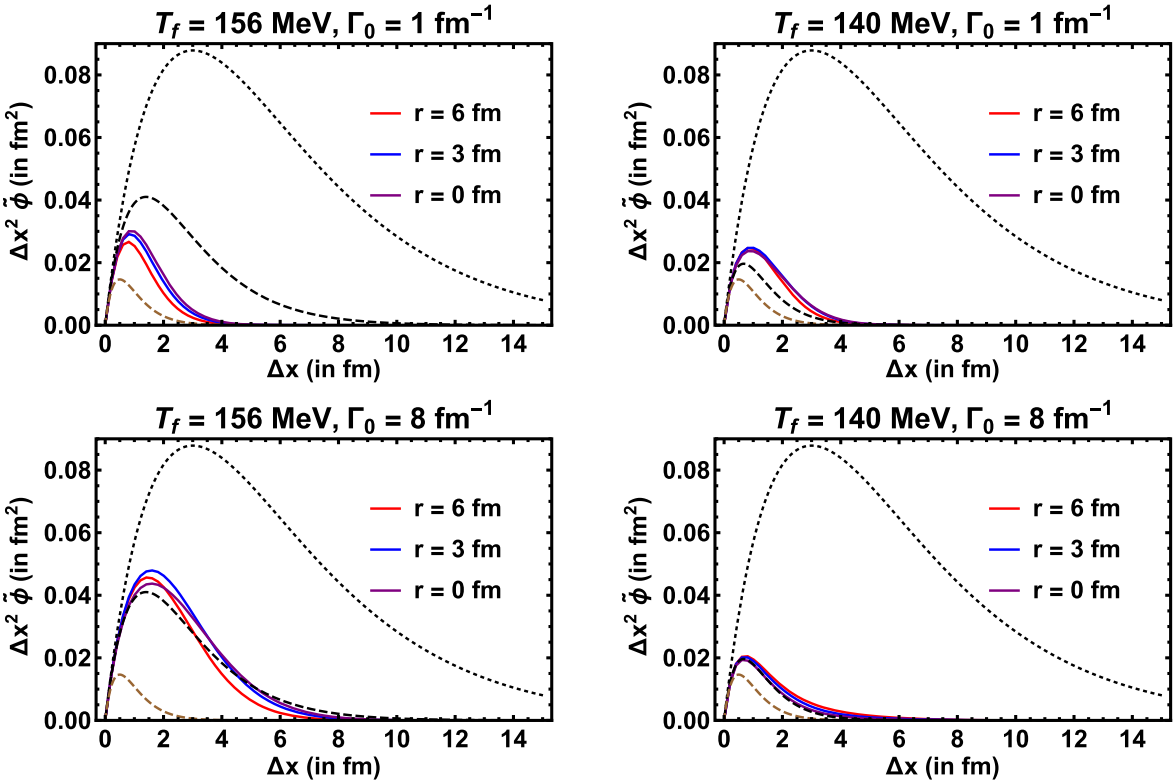

FIG. 19. $\tilde{\phi} \times \Delta x^2$, the measure of fluctuations of $\hat{s}$ described by the correlator $\langle \delta\hat{s}(x_+)\delta\hat{s}(x_-)\rangle$, at freeze-out as a function of the spatial separation between the points $\Delta x \equiv |\Delta \boldsymbol{x}_\perp|$. In the calculations depicted in different panels, the $\phi_{\boldsymbol{Q}}$'s were evolved with two different Γ_0's until freeze-out at two different T_f's, with the inverse Fourier transform to obtain $\tilde{\phi}(\boldsymbol{x}_\perp)$ performed at T_f. In all panels, we have chosen a trajectory with $\xi_{\max} = 3$ fm. The three r values depicted via the colored curves correspond to three r values on the freeze-out surface in the lab frame. The black dashed and dotted curves are the equilibrium curves at $T = T_f$ and $T = T_c$ respectively. The dashed brown curve is the (noncritical) equilibrium curve corresponding to $\xi = \xi_0$.

fluctuations in Fig. 19 is not affected by changing Γ_0, while at the same time the spatial correlator becomes longer ranged as Γ_0 is increased. The central difference between the model A dynamics here in Fig. 19 and the model H dynamics in Fig. 12 is that here $\tilde{\phi}(\Delta \boldsymbol{x}_\perp)$ is positive at large Δx: the fact that it becomes negative in the large Δx region in Fig. 12 is a direct consequence of conservation in model H.

3. Variance of particle multiplicities

As in Sec. IV, but here with model A dynamics, we close by computing and plotting the normalized fluctuation measure for protons and pions, $\tilde{\omega}_p$ and $\tilde{\omega}_\pi$, in Figs. 20 and 21. As in Figs. 13 and 14, to which these figures can be compared, these results demonstrate that for trajectories passing closer to the critical point (i.e., for trajectories with larger $\xi_{\max}$) the magnitude of fluctuations is larger. Again as in Sec. IV, the magnitude of the effect depends on the rate of the relaxation of the fluctuations, controlled here by parameter Γ_0. We see that for large enough values of Γ_0, e.g., 8 fm^{-1}, the proton and pion fluctuations are able to come reasonably close to their equilibrium values, which as an aside means that they depend quite sensitively on the freeze-out temperature. The differences that we discussed at length in Sec. IV originate from the effects of conservation.

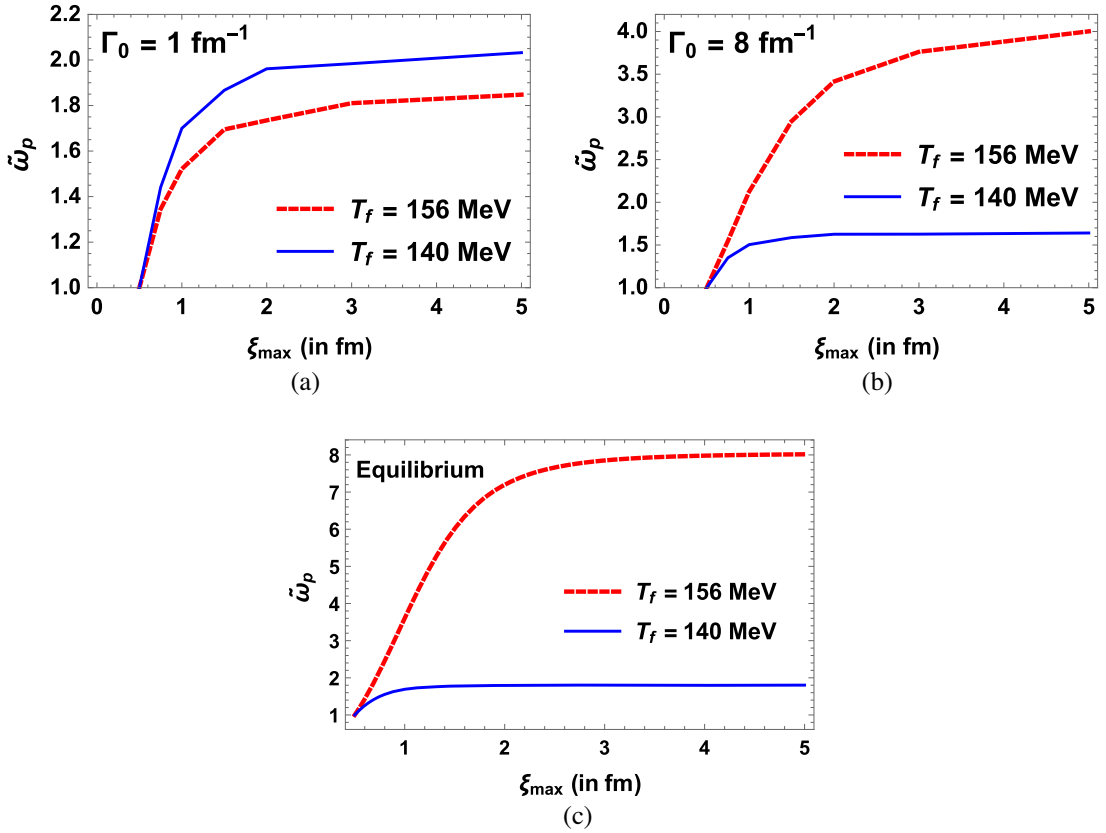

FIG. 20. Normalized measure of the fluctuations in proton multiplicity, $\tilde{\omega}_p = \frac{\omega_p}{\omega_p^{\rm nc}}$, as a function of the maximum equilibrium correlation length along the system trajectory, which is to say as a function of how closely the trajectory passes the critical point. As $\Gamma_0 \to \infty$, the $\tilde{\omega}_p$'s approach their equilibrium values shown in panel (c).

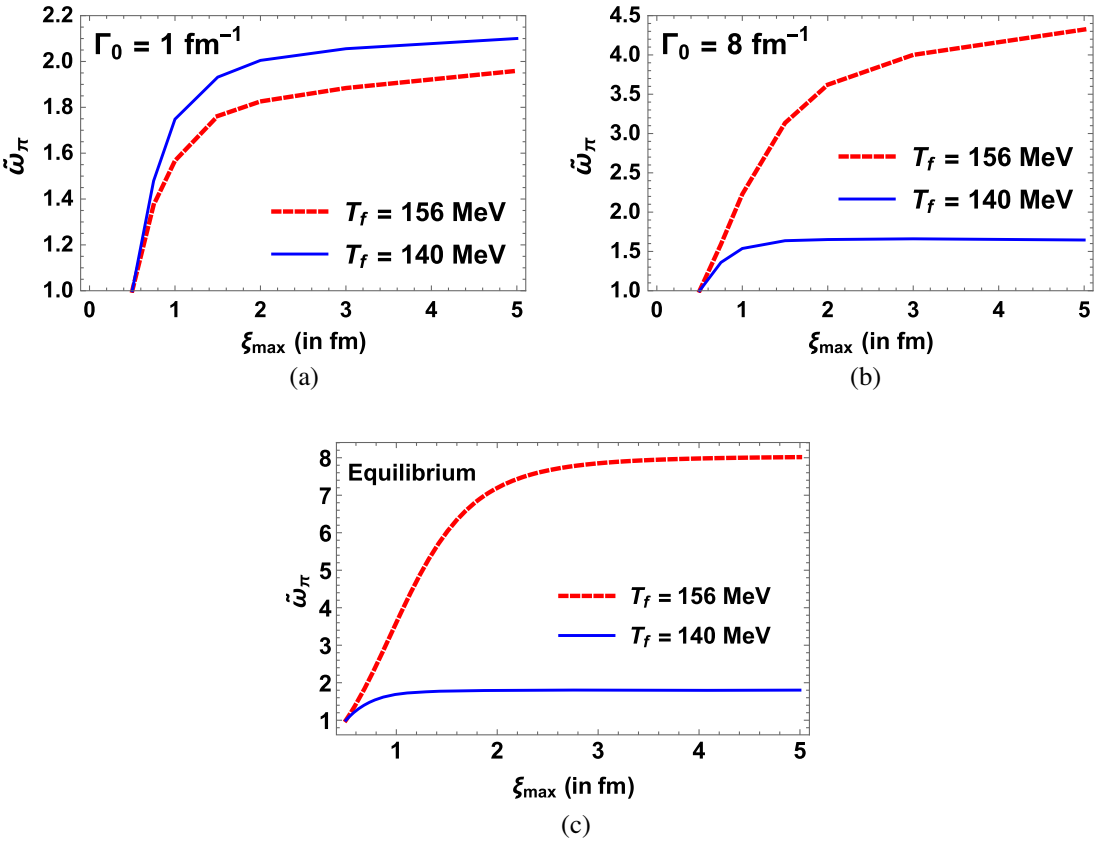

FIG. 21. Normalized measure of the fluctuations in pion multiplicity, $\tilde{\omega}_\pi = \frac{\omega_\pi}{\omega_\pi^{\rm eq}}$, as a function of the maximum equilibrium correlation length along the system trajectory, which is to say as a function of how closely the trajectory passes the critical point. As $\Gamma_0 \to \infty$, the $\tilde{\omega}_\pi$'s approach their equilibrium values shown in panel (c).

[1] A. Aprahamian *et al.*, Reaching for the horizon: The 2015 long range plan for nuclear science (2015), https://science.osti.gov/-/media/np/nsac/pdf/2015LRP/2015_LRPNS_091815.pdf.

[2] W. Busza, K. Rajagopal, and W. van der Schee, Heavy ion collisions: The big picture, and the big questions, Annu. Rev. Nucl. Part. Sci. **68**, 339 (2018).

[3] A. Bzdak, S. Esumi, V. Koch, J. Liao, M. Stephanov, and N. Xu, Mapping the phases of quantum chromodynamics with beam energy scan, Phys. Rep. **853**, 1 (2020).

[4] M. Abdallah *et al.* (STAR Collaboration), Cumulants and correlation functions of net-proton, proton and antiproton multiplicity distributions in Au + Au collisions at RHIC, Phys. Rev. C **104**, 024902 (2021).

[5] M. A. Stephanov, K. Rajagopal, and E. V. Shuryak, Signatures of the Tricritical Point in QCD, Phys. Rev. Lett. **81**, 4816 (1998).

[6] M. A. Stephanov, K. Rajagopal, and E. V. Shuryak, Event-by-event fluctuations in heavy ion collisions and the QCD critical point, Phys. Rev. D **60**, 114028 (1999).

[7] Y. Hatta and M. A. Stephanov, Proton Number Fluctuation as a Signal of the QCD Critical Endpoint, Phys. Rev. Lett. **91**, 102003 (2003); Erratum, Phys. Rev. Lett. **91**, 129901 (2003).

[8] M. A. Stephanov, Non-Gaussian Fluctuations Near the QCD Critical Point, Phys. Rev. Lett. **102**, 032301 (2009).

[9] M. Asakawa, S. Ejiri, and M. Kitazawa, Third Moments of Conserved Charges as Probes of QCD Phase Structure, Phys. Rev. Lett. **103**, 262301 (2009).

[10] C. Athanasiou, K. Rajagopal, and M. Stephanov, Using higher moments of fluctuations and their ratios in the search for the QCD critical point, Phys. Rev. D **82**, 074008 (2010).

[11] M. A. Stephanov, On the Sign of Kurtosis Near the QCD Critical Point, Phys. Rev. Lett. **107**, 052301 (2011).

[12] B. Ling and M. A. Stephanov, Acceptance dependence of fluctuation measures near the QCD critical point, Phys. Rev. C **93**, 034915 (2016).

[13] J. Brewer, S. Mukherjee, K. Rajagopal, and Y. Yin, Searching for the QCD critical point via the rapidity dependence of cumulants, Phys. Rev. C **98**, 061901 (2018).

[14] K. Rajagopal, G. Ridgway, R. Weller, and Y. Yin, Understanding the out-of-equilibrium dynamics near a critical point in the QCD phase diagram, Phys. Rev. D **102**, 094025 (2020).
[15] B. Berdnikov and K. Rajagopal, Slowing out-of-equilibrium near the QCD critical point, Phys. Rev. D **61**, 105017 (2000).
[16] S. Mukherjee, R. Venugopalan, and Y. Yin, Real time evolution of non-Gaussian cumulants in the QCD critical regime, Phys. Rev. C **92**, 034912 (2015).
[17] S. Mukherjee, R. Venugopalan, and Y. Yin, Universal Off-Equilibrium Scaling of Critical Cumulants in the QCD Phase Diagram, Phys. Rev. Lett. **117**, 222301 (2016).
[18] M. Stephanov and Y. Yin, Hydrodynamics with parametric slowing down and fluctuations near the critical point, Phys. Rev. D **98**, 036006 (2018).
[19] Y. Akamatsu, A. Mazeliauskas, and D. Teaney, A kinetic regime of hydrodynamic fluctuations and long time tails for a Bjorken expansion, Phys. Rev. C **95**, 014909 (2017).
[20] Y. Akamatsu, D. Teaney, F. Yan, and Y. Yin, Transits of the QCD critical point, Phys. Rev. C **100**, 044901 (2019).
[21] M. Bluhm and M. Nahrgang, Time-evolution of net-baryon density fluctuations across the QCD critical region, Springer Proc. Phys. **250**, 351 (2020).
[22] Y. Akamatsu, A. Mazeliauskas, and D. Teaney, Bulk viscosity from hydrodynamic fluctuations with relativistic hydrokinetic theory, Phys. Rev. C **97**, 024902 (2018).
[23] X. An, G. Başar, M. Stephanov, and H.-U. Yee, Relativistic hydrodynamic fluctuations, Phys. Rev. C **100**, 024910 (2019).
[24] M. Martinez and T. Schäfer, Stochastic hydrodynamics and long time tails of an expanding conformal charged fluid, Phys. Rev. C **99**, 054902 (2019).
[25] M. Martinez, T. Schäfer, and V. Skokov, Critical behavior of the bulk viscosity in QCD, Phys. Rev. D **100**, 074017 (2019).
[26] X. An, G. Başar, M. Stephanov, and H.-U. Yee, Fluctuation dynamics in a relativistic fluid with a critical point, Phys. Rev. C **102**, 034901 (2020).
[27] X. An, G. Başar, M. Stephanov, and H.-U. Yee, Evolution of Non-Gaussian Hydrodynamic Fluctuations, Phys. Rev. Lett. **127**, 072301 (2021).
[28] M. Bluhm *et al.*, Dynamics of critical fluctuations: Theory—phenomenology—heavy-ion collisions, Nucl. Phys. **A1003**, 122016 (2020).
[29] C. Shen and B. Schenke, Dynamical initial state model for relativistic heavy-ion collisions, Phys. Rev. C **97**, 024907 (2018).
[30] L. Du, U. Heinz, K. Rajagopal, and Y. Yin, Fluctuation dynamics near the QCD critical point, Phys. Rev. C **102**, 054911 (2020).
[31] X. An *et al.*, The BEST framework for the search for the QCD critical point and the chiral magnetic effect, Nucl. Phys. **A1017**, 122343 (2022).
[32] J. I. Kapusta, B. Muller, and M. Stephanov, Relativistic theory of hydrodynamic fluctuations with applications to heavy ion collisions, Phys. Rev. C **85**, 054906 (2012).
[33] K. Murase and T. Hirano, Relativistic fluctuating hydrodynamics with memory functions and colored noises, arXiv:1304.3243.
[34] C. Young, J. I. Kapusta, C. Gale, S. Jeon, and B. Schenke, Thermally fluctuating second-order viscous hydrodynamics and heavy-ion collisions, Phys. Rev. C **91**, 044901 (2015).
[35] K. Murase and T. Hirano, Hydrodynamic fluctuations and dissipation in an integrated dynamical model, Nucl. Phys. **A956**, 276 (2016).
[36] M. Singh, C. Shen, S. McDonald, S. Jeon, and C. Gale, Hydrodynamic fluctuations in relativistic heavy-ion collisions, Nucl. Phys. **A982**, 319 (2019).
[37] M. Nahrgang, M. Bluhm, T. Schäfer, and S. Bass, Toward the description of fluid dynamical fluctuations in heavy-ion collisions, Acta Phys. Pol. B Proc. Suppl. **10**, 687 (2017).
[38] M. Nahrgang, M. Bluhm, T. Schaefer, and S. A. Bass, Diffusive dynamics of critical fluctuations near the QCD critical point, Phys. Rev. D **99**, 116015 (2019).
[39] M. Nahrgang and M. Bluhm, Modeling the diffusive dynamics of critical fluctuations near the QCD critical point, Phys. Rev. D **102**, 094017 (2020).
[40] A. Sakai, K. Murase, and T. Hirano, Rapidity decorrelation of anisotropic flow caused by hydrodynamic fluctuations, Phys. Rev. C **102**, 064903 (2020).
[41] D. Schweitzer, S. Schlichting, and L. von Smekal, Critical dynamics of relativistic diffusion, arXiv:2110.01696.
[42] A. Florio, E. Grossi, A. Soloviev, and D. Teaney, Dynamics of the $O(4)$ critical point in QCD, Phys. Rev. D **105**, 054512 (2022).
[43] N. Abbasi and M. Kaminski, Characteristic momentum of Hydro+ and a bound on the speed of sound near the QCD critical point, Phys. Rev. D **106**, 016004 (2022).
[44] F. Cooper and G. Frye, Comment on the single particle distribution in the hydrodynamic and statistical thermodynamic models of multiparticle production, Phys. Rev. D **10**, 186 (1974).
[45] J. Berges and K. Rajagopal, Color superconductivity and chiral symmetry restoration at nonzero baryon density and temperature, Nucl. Phys. **B538**, 215 (1999).
[46] A. M. Halasz, A. D. Jackson, R. E. Shrock, M. A. Stephanov, and J. J. M. Verbaarschot, On the phase diagram of QCD, Phys. Rev. D **58**, 096007 (1998).
[47] R. Guida and J. Zinn-Justin, 3-D Ising model: The scaling equation of state, Nucl. Phys. **B489**, 626 (1997).
[48] J. Zinn-Justin, *Quantum Field Theory and Critical Phenomena*, International Series of Monographs on Physics Vol. 77 (Oxford University Press, New York, 2021).
[49] K. Rajagopal and F. Wilczek, Static and dynamic critical phenomena at a second order QCD phase transition, Nucl. Phys. **B399**, 395 (1993).
[50] K. Rajagopal and F. Wilczek, The condensed matter physics of QCD, in *At the Frontier of Particle Physics. Handbook of QCD. Vol. 1–3*, edited by M. Shifman and B. Ioffe (World Scientific, Singapore, 2000), pp. 2061–2151.
[51] P. Parotto, M. Bluhm, D. Mroczek, M. Nahrgang, J. Noronha-Hostler, K. Rajagopal, C. Ratti, T. Schäfer, and M. Stephanov, Lattice-QCD-based equation of state with a critical point, Phys. Rev. C **101**, 034901 (2020).
[52] M. S. Pradeep and M. Stephanov, Universality of the critical point mapping between Ising model and QCD at small quark mass, Phys. Rev. D **100**, 056003 (2019).

[53] D. T. Son and M. A. Stephanov, Dynamic universality class of the QCD critical point, Phys. Rev. D **70**, 056001 (2004).
[54] P. C. Hohenberg and B. I. Halperin, Theory of dynamic critical phenomena, Rev. Mod. Phys. **49**, 435 (1977).
[55] K. Kawasaki, Kinetic equations and time correlation functions of critical fluctuations, Ann. Phys. (N.Y.) **61**, 1 (1970).
[56] S. Borsanyi, Z. Fodor, C. Hoelbling, S. D. Katz, S. Krieg, and K. K. Szabo, Full result for the QCD equation of state with $2+1$ flavors, Phys. Lett. B **730**, 99 (2014).
[57] A. Bazavov *et al.* (HotQCD Collaboration), Equation of state in $(2+1)$-flavor QCD, Phys. Rev. D **90**, 094503 (2014).
[58] H. Grad, On the kinetic theory of rarefied gases, Commun. Pure Appl. Math. **2**, 331 (1949).
[59] J. Anderson and H. Witting, A relativistic relaxation-time model for the Boltzmann equation, Physica (Amsterdam) **74**, 466 (1974).
[60] S. Pratt and G. Torrieri, Coupling relativistic viscous hydrodynamics to Boltzmann descriptions, Phys. Rev. C **82**, 044901 (2010).
[61] M. McNelis, D. Everett, and U. Heinz, Particlization in fluid dynamical simulations of heavy-ion collisions: The i S3D module, Comput. Phys. Commun. **258**, 107604 (2021).
[62] M. McNelis and U. Heinz, Modified equilibrium distributions for Cooper–Frye particlization, Phys. Rev. C **103**, 064903 (2021).
[63] G. S. Denicol, C. Gale, S. Jeon, A. Monnai, B. Schenke, and C. Shen, Net baryon diffusion in fluid dynamic simulations of relativistic heavy-ion collisions, Phys. Rev. C **98**, 034916 (2018).
[64] L. Jiang, P. Li, and H. Song, Correlated fluctuations near the QCD critical point, Phys. Rev. C **94**, 024918 (2016).
[65] M. Bluhm, M. Nahrgang, S. A. Bass, and T. Schaefer, Impact of resonance decays on critical point signals in net-proton fluctuations, Eur. Phys. J. C **77**, 210 (2017).
[66] S. Wu, Z. Wu, and H. Song, Universal scaling of the σ field and net-protons from Langevin dynamics of model A, Phys. Rev. C **99**, 064902 (2019).
[67] M. Szymański, M. Bluhm, K. Redlich, and C. Sasaki, Net-proton number fluctuations in the presence of the QCD critical point, J. Phys. G **47**, 045102 (2020).
[68] M. A. Stephanov, Evolution of fluctuations near QCD critical point, Phys. Rev. D **81**, 054012 (2010).
[69] A. Bzdak, V. Koch, and V. Skokov, Baryon number conservation and the cumulants of the net proton distribution, Phys. Rev. C **87**, 014901 (2013).
[70] V. Vovchenko, R. V. Poberezhnyuk, and V. Koch, Cumulants of multiple conserved charges and global conservation laws, J. High Energy Phys. 10 (2020) 089.
[71] M. Luzum and H. Petersen, Initial state fluctuations and final state correlations in relativistic heavy-ion collisions, J. Phys. G **41**, 063102 (2014).
[72] S. Floerchinger and U. A. Wiedemann, Kinetic freeze-out, particle spectra and harmonic flow coefficients from mode-by-mode hydrodynamics, Phys. Rev. C **89**, 034914 (2014).
[73] J. D. Bjorken, Highly relativistic nucleus-nucleus collisions: The central rapidity region, Phys. Rev. D **27**, 140.
[74] Y. Ohnishi, M. Kitazawa, and M. Asakawa, Thermal blurring of event-by-event fluctuations generated by rapidity conversion, Phys. Rev. C **94**, 044905 (2016).
[75] R. Baier and P. Romatschke, Causal viscous hydrodynamics for central heavy-ion collisions, Eur. Phys. J. C **51**, 677 (2007).
[76] R. Baier, P. Romatschke, and U. A. Wiedemann, Dissipative hydrodynamics and heavy ion collisions, Phys. Rev. C **73**, 064903 (2006).
[77] P. Romatschke, Causal viscous hydrodynamics for central heavy-ion collisions. II. Meson spectra and HBT radii, Eur. Phys. J. C **52**, 203 (2007).